Bifurcations in nonlinear discontinuous systems

Bifurcations in Nonlinear Discontinuous Systems

R.I. Leine
B.L. van de Vrande
D.H. van Campen

16 March 1999
Report number: WFW 99.010

Internal Report

Authors: ir. R.I. Leine
ir. B.L. van de Vrande
Prof. Dr. ir. D.H. van Campen

Division of Computational and Experimental Mechanics
Department of Mechanical Engineering
Eindhoven University of Technology,
PO box 513, 5600 MB Eindhoven, The Netherlands

Bifurcations in Nonlinear Discontinuous Systems

R. I. Leine B. L. van de Vrande D. H. van Campen

Department of Mechanical Engineering,
Eindhoven University of Technology,
P. O. Box 513, 5600 MB Eindhoven, The Netherlands
E-mail : remco@wfw.wtb.tue.nl

Abstract

In this paper a theory for bifurcations of discontinuous systems is presented. First, Filippov's theory for the definition of solutions of discontinuous systems is surveyed. Furthermore, jumps in fundamental solution matrices are discussed. The paper treats discontinuous bifurcations of fixed points and periodic solutions. It is shown how jumps in the fundamental solution matrix lead to jumps of the Floquet multipliers of periodic solutions. The Floquet multipliers can jump through the unit circle causing discontinuous bifurcations. Numerical examples are treated which show various discontinuous bifurcations. Also infinitely unstable solutions are addressed.

1 Introduction

The objective of this paper is to present a new theory for bifurcations of discontinuous systems. During the last decade many textbooks about bifurcation theory for smooth systems appeared and bifurcations of smooth vector fields are well understood [8, 9, 12, 25]. However, little is known about bifurcations of discontinuous vector fields. Discontinuous dynamical systems arise due to physical discontinuities such as dry friction, impact and backlash in mechanical systems or diode elements in electrical circuits. Many papers deal with discontinuous systems [6, 10, 11, 22, 23, 26, 27, 28]. Published bifurcation diagrams constructed from data obtained by brute force techniques only show stable branches, whereas those made by path-following techniques do show bifurcations to unstable solutions but the bifurcations behave smoothly and are not discontinuous.

Andronov et al. [2] treat periodic solutions of discontinuous systems. They revealed many aspects of discontinuous systems but did not treat discontinuous bifurcations with regard to Floquet theory.

The current paper presents a new bifurcation theory, which starts with Filippov's theory, explains how the bifurcations come into being through jumps of the fundamental solution matrix and shows how discontinuous bifurcations are related to continuous bifurcations.

The theory of Filippov is briefly discussed in Section 2. This theory gives a generalized definition of the solution of differential equations with a discontinuous right-hand side.

In Section 3 fundamental solution matrices of discontinuous systems are discussed. Discontinuities of the vector field cause jumps in the fundamental solution matrix.

Section 5 discusses a linear approximation which approximates a discontinuous system by a stiff continuous system or a non-smooth system by a smooth system.

Section 6 deals with bifurcations of fixed points of non-smooth continuous systems. Bifurcations of fixed points of non-smooth systems help to give insight in bifurcations of periodic solutions of discontinuous systems. We restrict ourselves to local codimension-1 bifurcations. The saddle-node, transcritical, pitchfork and Hopf bifurcations are discussed. Theorems for the existence of discontinuous bifurcations of fixed points are given.

How bifurcations of periodic solutions of discontinuous systems come into being is explained in Section 7. A comparison is made between continuous bifurcations in smooth systems and discontinuous bifurcations. Two examples are discussed which show discontinuous fold bifurcations

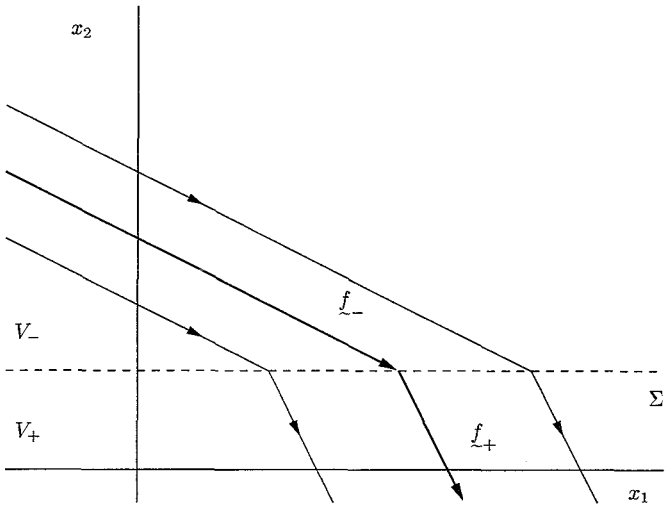

Figure 2.1: Transversal intersection

systems, e.a. a trilinear system which shows a discontinuous fold bifurcation (Section 7.2) and a stick-slip model which shows a discontinuous fold bifurcation bifurcation to an infinitely unstable branch (Section 7.3). The discontinuous symmetry-breaking bifurcation will be discussed in Section 8. The discontinuous flip bifurcation in Section 9 can be described by the tent map.

Section 10 gives conclusions.

2 Filippov's theory

2.1 The construction of a solution

A dynamical system is usually expressed as the following set of ordinary differential equations

$$\dot{\underset{\sim}{x}}(t) = \underset{\sim}{f}(t, \underset{\sim}{x}(t)) \tag{2.1}$$

where $\underset{\sim}{x}$ is the state vector and $\underset{\sim}{f}(t, \underset{\sim}{x}(t))$ is the right-hand side describing the time derivative of the state vector. If the vector field is smooth, that is $\underset{\sim}{f}$ is continuously differentiable, then the solution of the system in Equation 2.1 exists and is unique. We say that the vector field $\underset{\sim}{f}$ generates a *flow* which is the solution of the set of differential equations.

However, differential equations stemming from physical systems may be non-smooth. The right-hand side can be discontinuous while the flow remains continuous. The theory of Filippov [5] gives a generalized definition of the solution of differential equations which incorporates systems with a discontinuous right-hand side. The Filippov theory will be briefly outlined in this section.

Consider the nonlinear system with discontinuous right-hand side

$$\dot{\underset{\sim}{x}}(t) = \underset{\sim}{f}(t, \underset{\sim}{x}(t)) = \begin{cases} \underset{\sim}{f}_-(t, \underset{\sim}{x}(t)) & \underset{\sim}{x} \in V_- \\ \underset{\sim}{f}_+(t, \underset{\sim}{x}(t)) & \underset{\sim}{x} \in V_+, \end{cases} \tag{2.2}$$

with the initial condition

$$\underset{\sim}{x}(t=0) = \underset{\sim}{x}_0. \tag{2.3}$$

Let $\underset{\sim}{f}$ be discontinuous but such that it is piecewise continuous on V_- and V_+. Let Σ be the hyper-surface between the subspaces V_- and V_+.

Consider the vector field of Figure 2.1 where the vector field is converging to Σ in the space V_- and diverging in the space V_+. A flow with an initial condition in V_- will after some time hit

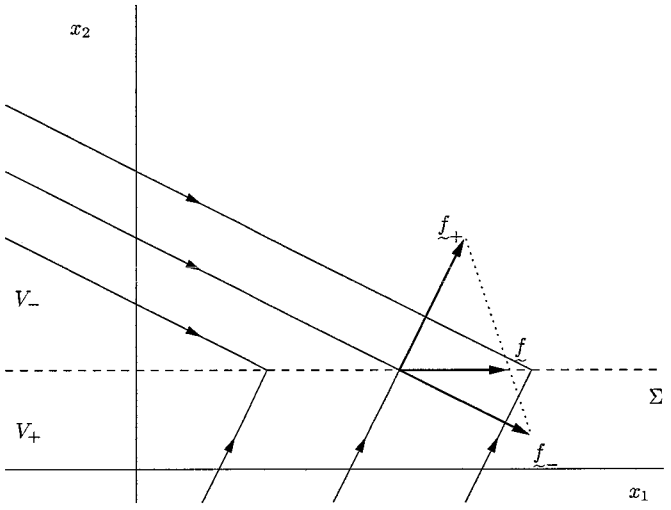

Figure 2.2: Attraction sliding mode

Σ, cross it transversally and proceed in V_+. This is called a transversal intersection. The solution exists and is unique.

The vector field could also be converging in both V_- and V_+ to Σ. (Figure 2.2). The flow will hit Σ but cannot leave it. Thus the flow will move along the plane Σ. This is often called *sliding mode*. Let $\underset{\sim}{n}^T\underset{\sim}{f}_-$ and $\underset{\sim}{n}^T\underset{\sim}{f}_+$ be the projections of $\underset{\sim}{f}_-$ and $\underset{\sim}{f}_+$ on the normal to the hyperplane Σ. During the sliding mode the flow will proceed along Σ with time derivative $\underset{\sim}{f}$ given by

$$\underset{\sim}{f} = \alpha\underset{\sim}{f}_+ + (1-\alpha)\underset{\sim}{f}_- \tag{2.4}$$

with

$$\alpha = \frac{\underset{\sim}{n}^T\underset{\sim}{f}_-}{\underset{\sim}{n}^T(\underset{\sim}{f}_- - \underset{\sim}{f}_+)} \tag{2.5}$$

The solution of the attracting sliding mode exists and is unique.

The third possible case is depicted in Figure 2.3. Here the flows are diverging from Σ. A flow which starts close to Σ will move away from it. But a flow emanating on Σ can stay on Σ, obeying Filippov's solution, or leave Σ by entering V_- or V_+. Thus a flow with initial condition on Σ has three possible solutions. The solution still exists but is not unique.

Filippov's theory will turn out to be very important to understand infinitely unstable branches of stick-slip systems as will be pointed out in the next sections.

2.2 Numerical approximation

The vector field of Figure 2.4 pushes the flow which starts in point A to the hyperplane Σ at point B. The flow then slides along Σ and leaves Σ when the vector field in the space V_+ becomes parallel to Σ. The flow will then bend off at point C and reaches point D. This scenario is the attraction sliding mode. The flow from A to D is unique. If we consider the flow in backward time, that is from D to A, then the vector field reverses and the sliding mode will be of the repulsion type. Thus the reverse flow is not unique. This insight is essential to understand bifurcations of periodic solutions which have sliding modes which will be treated in the next sections.

If we try to integrate such a scenario numerically we are faced with a difficulty: a Runge-Kutta algorithm, for example, will have collocation points in both V_- and V_+ between B and C. It will find the correct solution but will take an enormous amounts of integration points.

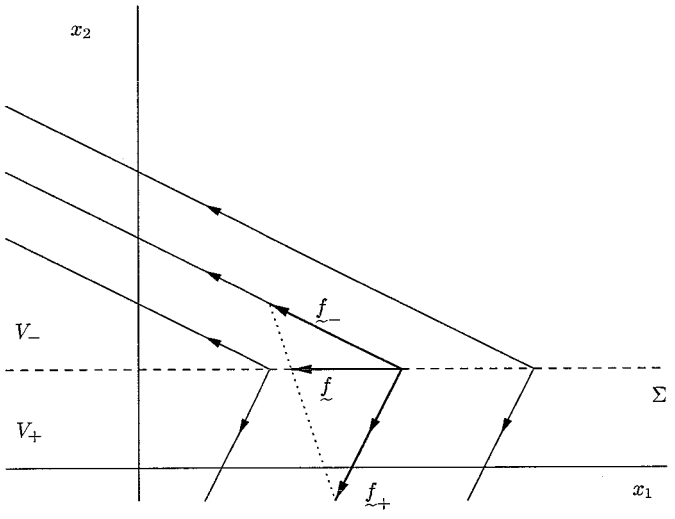

Figure 2.3: Repulsion sliding mode

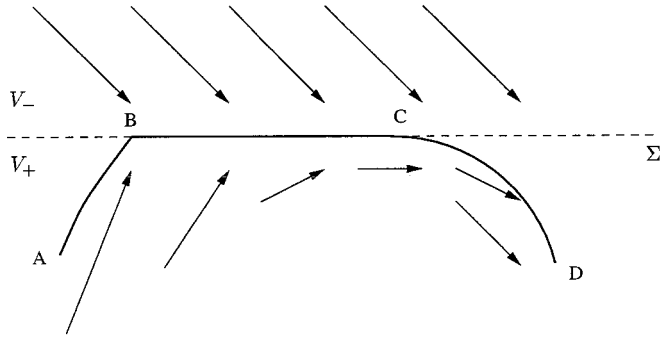

Figure 2.4: Exact sliding mode

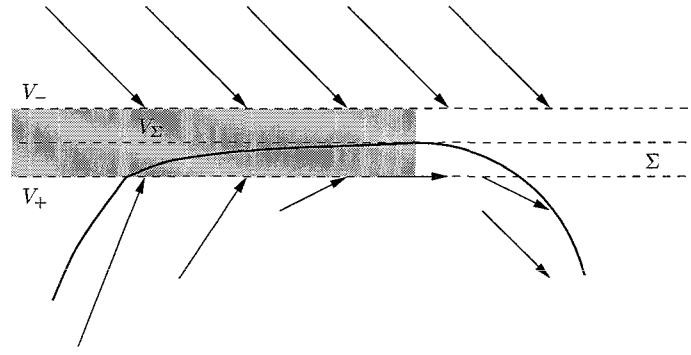

Figure 2.5: Numerical approximation

Instead, we construct a 'band' around Σ, namely the space V_Σ, to allow for an efficient numerical approximation. In the space V_Σ, the vector field is such that the flow is pushed to the middle of the band, thus to Σ. The space V_Σ ends when the vector field V_+ or V_- becomes parallel to Σ. The width of V_Σ should be taken small to yield a good approximation.

As an alternative, one can replace the discontinuous vector field by a smoothed vector field. However, the smoothing method yields stiff differential equations which are expensive to solve. The method proposed here is far more efficient as is pointed out in Leine et al. [13] where the two methods are compared.

3 Fundamental solution matrices

3.1 Introduction

The concept of a fundamental solution matrix is important in the stability analysis of periodic solutions of dynamical systems. The eigenvalues of the fundamental solutions matrix are called *Floquet multipliers* [8, 18, 19, 21]. Each Floquet multiplier provides a measure of the local orbital divergence or convergence along a particular direction over one period of the closed orbit. The Floquet multipliers thus determine the stability of the periodic motion.

Fundamental solution matrices are furthermore used in shooting methods for finding periodic solutions, in continuation methods to follow branches of periodic solutions, and they are used in the determination of Lyapunov exponents.

For continuous systems the fundamental solution matrix can be obtained in an elegant manner by integrating the so-called variational equation [3, 21]. Discontinuous systems however, exhibit discontinuities (or 'saltations'/'jumps') in the time evolution of the fundamental solution matrix.

The jumps in the fundamental solution matrix can be computed analytically by means of the theory of Aizerman and Gantmakher, which will be discussed in subsections 3.2 and 3.3. The Aizerman-Gantmakher theory will be extended in section 3.4 with the concept of a *conversion matrix*. The conversion matrix will show to be a useful property if one wants to compute the fundamental solution matrix first without accounting for the jumps and use this result to obtain the fundamental solution matrix with jumps being taken into account. It is especially useful for the discussion of discontinuous bifurcations of periodic solutions where the flow before the bifurcation does not cross the discontinuity but after the discontinuity does (Section 7).

The extended method is also suitable for the application of standard integration algorithms which do not have the feature to stop at state events.

The theory of Aizerman and Gantmakher was used by Bockman [4] and Müller [15] to calculate Lyapunov exponents of discontinuous systems.

3.2 Jumping conditions: A single discontinuity

Consider the nonlinear system with discontinuous right-hand side

$$\dot{\underset{\sim}{x}}(t) = \underset{\sim}{f}(t, \underset{\sim}{x}(t)) = \begin{cases} \underset{\sim}{f}_-(t, \underset{\sim}{x}(t)) & \underset{\sim}{x} \in V_- \\ \underset{\sim}{f}_+(t, \underset{\sim}{x}(t)) & \underset{\sim}{x} \in V_+, \end{cases} \tag{3.1}$$

with the initial condition

$$\underset{\sim}{x}(t = 0) = \underset{\sim}{x}_0. \tag{3.2}$$

Let $\underset{\sim}{f}$ be discontinuous but such that it is piecewise continuous on V_- and V_+. Let Σ be the hyper-surface between the subspaces V_- and V_+. An indicator function $h(t, \underset{\sim}{x}(t))$ defines the instant of discontinuity. The state crosses the discontinuity if it crosses the hyper-surface Σ defined by:

$$h(t, \underset{\sim}{x}(t)) = 0. \tag{3.3}$$

Then, the normal $\underset{\sim}{n}$ perpendicular to the surface Σ is given by

$$\underset{\sim}{n} = \underset{\sim}{n}(t, \underset{\sim}{x}(t)) = \text{grad}(h(t, \underset{\sim}{x}(t))). \tag{3.4}$$

At a certain point in time, say t_p, the flow $\underset{\sim}{x}$ will cross Σ, thus $h(t_p, \underset{\sim}{x}(t_p)) = 0$. At this discontinuity there are two derivatives $\underset{\sim p-}{f}$ and $\underset{\sim p+}{f}$ which lie in the direction of the flow as denoted in Figure 3.1. The derivatives have components $\underset{\sim p-}{f}^{\text{N}}$ and $\underset{\sim p+}{f}^{\text{N}}$ perpendicular to the hyper-surface and with magnitudes $\underset{\sim}{n}^T \underset{\sim p-}{f}$ and $\underset{\sim}{n}^T \underset{\sim p+}{f}$. We first consider only transversal intersections, where existence and uniqueness of the solution are assured (sliding mode problems will be treated later in this paper). In order to assure a transversal intersection, we assume that the projections of the derivatives $\underset{\sim p-}{f}$ and $\underset{\sim p+}{f}$ on the normal $\underset{\sim}{n}$ have the same sign

$$\underset{\sim}{n}^T \underset{\sim p-}{f} \underset{\sim}{n}^T \underset{\sim p+}{f} > 0. \tag{3.5}$$

Equation 3.5 assures that the flow leaves the hyper-surface and stays on the hyper-surface at one point of time and not on an interval of time (i.e. the flow *crosses* the hyper-surface).

A disturbance $\delta \underset{\sim}{x}_0$ on the initial condition will cause a disturbance $\delta \underset{\sim}{x}(t)$ on the state $\underset{\sim}{x}(t)$. The fundamental solution matrix $\underline{\Phi}(t, t_0)$ relates $\delta \underset{\sim}{x}(t)$ to $\delta \underset{\sim}{x}_0$,

$$\delta \underset{\sim}{x}(t) = \underline{\Phi}(t, t_0) \delta \underset{\sim}{x}_0. \tag{3.6}$$

The dependence of $\underline{\Phi}(t, t_0)$ on $\underset{\sim}{x}_0$ has been omitted for brevity. Let the flow start in the subspace V_-, that is $\underset{\sim}{x}_0 \in V_-$. Suppose the flow crosses the hyper-surface Σ at $t = t_p$, thus $h(t_p, \underset{\sim}{x}(t_p)) = 0$. The system is continuous on the interval $D = \{t \in I\!R \mid t_0 \leq t \leq t_p\}$. The fundamental solution matrix will also be continuous on the interior of D.

$$\lim_{t \uparrow t_z} \underline{\Phi}(t, t_0) = \lim_{t \downarrow t_z} \underline{\Phi}(t, t_0) = \underline{\Phi}(t_z, t_0), \qquad t_z \in D \tag{3.7}$$

The time evolution of the fundamental solution matrix on D can be obtained from the initial value problem

$$\dot{\underline{\Phi}}(t, t_0) = \frac{\partial \underset{\sim}{f}}{\partial \underset{\sim}{x}} \underline{\Phi}(t, t_0), \qquad \underline{\Phi}(t_0, t_0) = \underline{\Phi}_0 = \underline{I}. \tag{3.8}$$

This equation is called the *variational equation* [21].

The flow enters the subspace V_+ at $t = t_p$, and traverses V_+ during the interval $G = \{t \in I\!R \mid t_p \leq t \leq t_q\}$. The state vector $\underset{\sim}{x}(t_p)$ is located on the discontinuity and the Jacobian is therefore

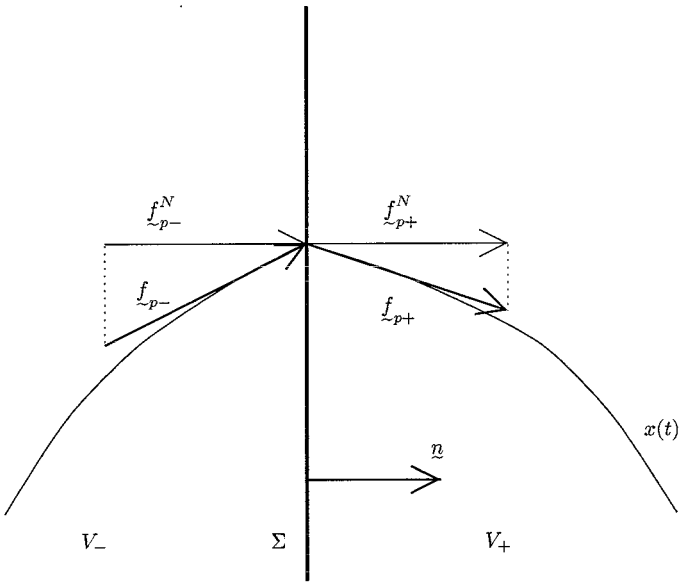

Figure 3.1: Projection of derivatives on the normal.

undefined at this point. The fundamental solution matrix $\underline{\Phi}(t, t_0)$ can exhibit a discontinuity at $t = t_p$. The following notation will be used:

$$\underline{\Phi}(t_{p-}, t_0) = \lim_{t \uparrow t_p} \underline{\Phi}(t, t_0), \qquad \underline{\Phi}(t_{p+}, t_0) = \lim_{t \downarrow t_p} \underline{\Phi}(t, t_0). \tag{3.9}$$

In general $\underline{\Phi}(t_{p-}, t_0) \neq \underline{\Phi}(t_{p+}, t_0)$. On D the fundamental solution matrix can be obtained from integrating the variational equation.

$$\underline{\Phi}(t_{p-}, t_0) = \int_{t_0}^{t_p} \dot{\underline{\Phi}}(t, t_0) dt + \underline{I} \tag{3.10}$$

On G the fundamental solution matrix can be constructed from ($t_q \in G$):

$$\underline{\Phi}(t_q, t_0) = \underline{\Phi}(t_q, t_{p+}) \underline{\Phi}(t_{p+}, t_0) = \left(\int_{t_p}^{t_q} \dot{\underline{\Phi}}(t, t_0) dt + \underline{I} \right) \underline{\Phi}(t_{p+}, t_0) \tag{3.11}$$

We now define a *saltation matrix* (or 'jump' matrix) $\underline{S}$ which maps $\underline{\Phi}(t_{p-}, t_0)$ to $\underline{\Phi}(t_{p+}, t_0)$

$$\underline{\Phi}(t_{p+}, t_0) = \underline{S}\, \underline{\Phi}(t_{p-}, t_0), \tag{3.12}$$

so that $\underline{S} = \underline{\Phi}(t_{p+}, t_{p-})$. Substitution of Equation 3.12 in Equation 3.11 yields

$$\underline{\Phi}(t_q, t_0) = \underline{\Phi}(t_q, t_{p+}) \underline{S}\, \underline{\Phi}(t_{p-}, t_0). \tag{3.13}$$

The construction of saltation matrices (or jump conditions) is due to Aizerman and Gantmakher [1].

3.3 Construction of Saltation Matrices

One question has not been answered up to now: how do we obtain the saltation matrix $\underline{S}$? The saltation matrix will be derived by inspecting the nonlinear dynamic system in the neighborhood of the action of a discontinuity. Consider the disturbed and undisturbed flow depicted in Figure 3.2.

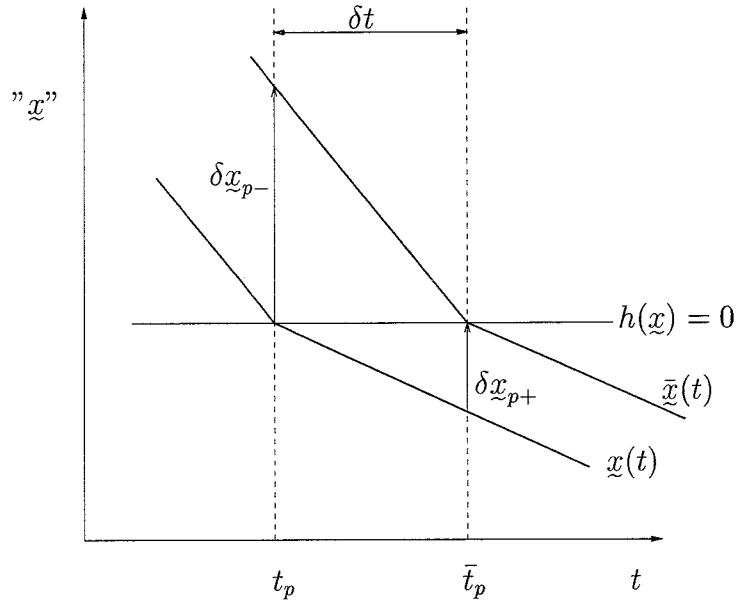

Figure 3.2: Disturbed and undisturbed flow.

Time is on the horizontal axis of Figure 3.2 and an arbitrary norm of $\underset{\sim}{x}$ is on the vertical axis. The disturbed flow $\bar{\underset{\sim}{x}}(t)$ is due to an initial disturbance

$$\bar{\underset{\sim}{x}}_0 = \underset{\sim}{x}_0 + \delta \underset{\sim}{x}_0. \tag{3.14}$$

The disturbed flow stays $\delta t = \bar{t}_p - t_p$ longer in V_- before hitting the hyper-surface Σ. The differences between the disturbed and undisturbed flows at the crossings are denoted by

$$\delta \underset{\sim}{x}_{p-} = \bar{\underset{\sim}{x}}(t_p) - \underset{\sim}{x}(t_p), \tag{3.15}$$

$$\delta \underset{\sim}{x}_{p+} = \bar{\underset{\sim}{x}}(\bar{t}_p) - \underset{\sim}{x}(\bar{t}_p). \tag{3.16}$$

We can express the undisturbed and disturbed flows in a first-order Taylor expansion

$$\underset{\sim}{x}(\bar{t}_p) \approx \underset{\sim}{x}(t_p) + \underset{\sim}{f}_{p+} \delta t, \tag{3.17}$$

$$\bar{\underset{\sim}{x}}(\bar{t}_p) \approx \underset{\sim}{x}(t_p) + \delta \underset{\sim}{x}_{p-} + \underset{\sim}{f}_{p-} \delta t. \tag{3.18}$$

The Equations 3.17 and 3.18 are inserted into Equation 3.16

$$\begin{aligned} \delta \underset{\sim}{x}_{p+} &= \bar{\underset{\sim}{x}}(\bar{t}_p) - \underset{\sim}{x}(\bar{t}_p) \\ &\approx \underset{\sim}{x}(t_p) + \delta \underset{\sim}{x}_{p-} + \underset{\sim}{f}_{p-} \delta t - (\underset{\sim}{x}(t_p) + \underset{\sim}{f}_{p+} \delta t) \\ &\approx \delta \underset{\sim}{x}_{p-} + \underset{\sim}{f}_{p-} \delta t - \underset{\sim}{f}_{p+} \delta t \end{aligned} \tag{3.19}$$

The disturbed flow satisfies the indicator function Equation 3.3. We apply a Taylor series expansion up to the first-order terms [15]:

$$\begin{aligned} 0 &= h(\bar{t}_p, \bar{\underset{\sim}{x}}(\bar{t}_p)) \\ &\approx h(t_p + \delta t, \underset{\sim}{x}(t_p) + \delta \underset{\sim}{x}_{p-} + \underset{\sim}{f}_{p-} \delta t) \\ &\approx \underbrace{h(t_p, \underset{\sim}{x}(t_p))}_{=0} + \underset{\sim}{n}^T (\delta \underset{\sim}{x}_{p-} + \underset{\sim}{f}_{p-} \delta t) + \frac{\partial h}{\partial t}(t_p, \underset{\sim}{x}(t_p)) \delta t \\ &\approx \underset{\sim}{n}^T (\delta \underset{\sim}{x}_{p-} + \underset{\sim}{f}_{p-} \delta t) + \frac{\partial h}{\partial t}(t_p, \underset{\sim}{x}(t_p)) \delta t, \end{aligned} \tag{3.20}$$

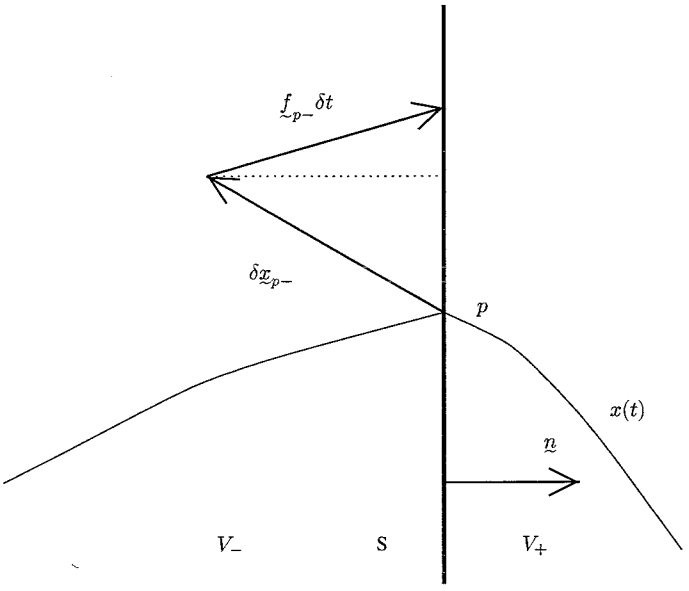

Figure 3.3: Construction of δt for autonomous Σ.

where the normal $\underset{\sim}{n}$ is defined by Equation 3.4.

From Equation 3.20 we can express the variation δt in terms of $\delta\underset{\sim}{x}_{p-}$.

$$\delta t = -\frac{\underset{\sim}{n}^T \delta\underset{\sim}{x}_{p-}}{\underset{\sim}{n}^T \underset{\sim}{f}_{p-} + \frac{\partial h}{\partial t}(t_p, \underset{\sim}{x}(t_p))} \tag{3.21}$$

For autonomous systems, the hyper-surface Σ does not depend on time, which simplifies the results as $\frac{\partial h}{\partial t}(t_p, \underset{\sim}{x}(t_p)) = 0$. In this case, the dependence between the variation δt and $\delta\underset{\sim}{x}_{p-}$ can be envisaged from Figure 3.3. Due to the variation $\delta\underset{\sim}{x}_{p-}$ the disturbed flow after a time t_p does not lie exactly on the (fixed) surface Σ. The disturbed flow has to stay a time δt longer in V_-, covering an additional distance $\underset{\sim}{f}_{p-}\delta t$, to reach Σ. The variation δt can be expressed as

$$\delta t = -\frac{\underset{\sim}{n}^T \delta\underset{\sim}{x}_{p-}}{\underset{\sim}{n}^T \underset{\sim}{f}_{p-}}. \tag{3.22}$$

Combining Equations 3.19 and Equation 3.21 gives

$$\delta\underset{\sim}{x}_{p+} = \delta\underset{\sim}{x}_{p-} + (\underset{\sim}{f}_{p+} - \underset{\sim}{f}_{p-})\frac{\underset{\sim}{n}^T \delta\underset{\sim}{x}_{p-}}{\underset{\sim}{n}^T \underset{\sim}{f}_{p-} + \frac{\partial h}{\partial t}(t_p, \underset{\sim}{x}(t_p))}. \tag{3.23}$$

We have now expressed the variation $\delta\underset{\sim}{x}_{p+}$ in the variation $\delta\underset{\sim}{x}_{p-}$. The saltation matrix relates $\delta\underset{\sim}{x}_{p+}$ to $\delta\underset{\sim}{x}_{p-}$

$$\delta\underset{\sim}{x}_{p+} = \underline{S}\delta\underset{\sim}{x}_{p-}, \tag{3.24}$$

thus we obtain the saltation matrix $\underline{S} = \underline{\Phi}(t_{p+}, t_{p-})$ as

$$\underline{S} = \underline{I} + \frac{(\underset{\sim}{f}_{p+} - \underset{\sim}{f}_{p-})\underset{\sim}{n}^T}{\underset{\sim}{n}^T \underset{\sim}{f}_{p-} + \frac{\partial h}{\partial t}(t_p, \underset{\sim}{x}(t_p))}. \tag{3.25}$$

The inverse of the saltation matrix $\underline{S}^{-1} = \underline{\Phi}(t_{p-}, t_{p+})$ is given by (for non-singular $\underline{S}$)

$$\underline{S}^{-1} = \underline{I} + \frac{(\underset{\sim}{f}_{p-} - \underset{\sim}{f}_{p+})\underset{\sim}{n}^T}{\underset{\sim}{n}^T \underset{\sim}{f}_{p+} + \frac{\partial h}{\partial t}(t_p, \underset{\sim}{x}(t_p))}. \tag{3.26}$$

3.4 Extension of the theory of Aizerman and Gantmakher

For continuous systems it is numerically convenient to integrate $\underset{\sim}{x}$ and the fundamental solution matrix simultaneously in a combined system:

$$\begin{bmatrix} \dot{\underset{\sim}{x}} \\ \dot{\underline{\Phi}} \end{bmatrix} = \begin{bmatrix} \underset{\sim}{f}(t, \underset{\sim}{x}) \\ \frac{\partial \underset{\sim}{f}}{\partial \underset{\sim}{x}} \underline{\Phi} \end{bmatrix} \qquad \text{(continuous)} \tag{3.27}$$

However, for a discontinuous system one cannot obtain the fundamental solution matrix directly. Instead we define the *unwrapped fundamental solution matrix* $\underline{\Phi}_U(t, t_0)$ by its variational equation

$$\dot{\underline{\Phi}}_U(t, t_0) = \frac{\partial \underset{\sim}{f}^*}{\partial \underset{\sim}{x}} \underline{\Phi}_U(t, t_0), \qquad \underline{\Phi}_U(t_0, t_0) = \underline{I}, \tag{3.28}$$

where $\partial \underset{\sim}{f}^* / \partial \underset{\sim}{x}$ is the special Jacobian defined by

$$\frac{\partial \underset{\sim}{f}^*}{\partial \underset{\sim}{x}} (t_z, \underset{\sim}{x}(t_z)) = \begin{cases} \frac{\partial \underset{\sim}{f}}{\partial \underset{\sim}{x}}(t_z, \underset{\sim}{x}(t_z)) & h(t_z, \underset{\sim}{x}(t_z)) \neq 0 \\ \lim_{t \uparrow t_z} \frac{\partial \underset{\sim}{f}}{\partial \underset{\sim}{x}}(t, \underset{\sim}{x}(t)) & h(t_z, \underset{\sim}{x}(t_z)) = 0 \end{cases} \tag{3.29}$$

While the Jacobian does not exist at the discontinuity, the special Jacobian does. Regarding the calculation of $\underline{\Phi}_U$, it does not matter which value is taken for $\partial \underset{\sim}{f}^* / \partial \underset{\sim}{x}$ at the discontinuity, as $h(t_z, \underset{\sim}{x}(t_z)) = 0$ only at one point in time and not on an interval due to Equation 3.5. The value for $\partial \underset{\sim}{f}^* / \partial \underset{\sim}{x}$ at $h(t_z, \underset{\sim}{x}(t_z)) = 0$ is thus arbitrary but must exist and be finite and is taken to be the left limit. However, the indicator function will most likely not be exactly zero in digital computation. For continuous systems $\underline{\Phi}_U = \underline{\Phi}$ holds. On D the unwrapped fundamental solution matrix is equal to the fundamental solution matrix.

$$\underline{\Phi}_U(t, t_0) = \underline{\Phi}(t, t_0) \quad t \in D \tag{3.30}$$

Thus $\underline{\Phi}(t_{p-}, t_0) = \underline{\Phi}_U(t_p, t_0)$. On G the unwrapped fundamental solution matrix is not affected by $\underline{S}$

$$\underline{\Phi}_U(t, t_0) = \underline{\Phi}(t, t_{p+}) \underline{\Phi}(t_{p-}, t_0) \quad t \in G \tag{3.31}$$

Matrix manipulation yields $\underline{\Phi}(t, t_{p+})$ [1]

$$\underline{\Phi}(t, t_{p+}) = \underline{\Phi}_U(t, t_0) \underline{\Phi}^{-1}(t_{p-}, t_0) = \underline{\Phi}_U(t, t_0) \underline{\Phi}_U^{-1}(t_p, t_0) \tag{3.32}$$

We are now able to express the fundamental solution matrix in the unwrapped fundamental solution matrix and the saltation matrix.

$$\begin{aligned} \underline{\Phi}(t, t_0) &= \underline{\Phi}(t, t_{p+}) \underline{S} \, \underline{\Phi}(t_{p-}, t_0) \\ &= \underline{\Phi}_U(t, t_0) \underline{\Phi}_U^{-1}(t_p, t_0) \underline{S} \, \underline{\Phi}_U(t_p, t_0) \\ &= \underline{\Phi}_U(t, t_0) \underline{C}(t, t_0) \end{aligned} \tag{3.33}$$

We call $\underline{C}(t, t_0)$ the *conversion matrix.*

3.5 Multiple discontinuities

We discussed the conversion matrix for a single discontinuity. We now discuss the conversion matrix for two discontinuities. We split the time interval $W = \{t \in \boldsymbol{R} \mid t_0 \leq t \leq t_0 + T\}$ in two subintervals $W_\alpha = \{t \in \boldsymbol{R} \mid t_0 \leq t \leq t_c\}$ and $W_\beta = \{t \in \boldsymbol{R} \mid t_c \leq t \leq t_0 + T\}$. Let the

[1] Remark : $\underline{\Phi}_U(t_p, t_0)$ is non-singular as it is not affected by $\underline{S}$.

system posses a discontinuity at $t = t_\alpha$, $t_\alpha \in W_\alpha$, and at $t = t_\beta$, $t_\beta \in W_\alpha$. We now construct the fundamental solution matrix from

$$\begin{aligned} \underline{\Phi}(t_0 + T, t_0) &= \underline{\Phi}(t_0 + T, t_c)\underline{\Phi}(t_c, t_0) \\ &= \underline{\Phi}_U(t_0 + T, t_c)\underline{C}_\beta(t_0 + T, t_c)\underline{\Phi}_U(t_c, t_0)\underline{C}_\alpha(t_c, t_0) \end{aligned} \tag{3.34}$$

We now substitute the relations for the conversion matrices

$$\underline{\Phi}(t_0 + T, t_0) = \underline{\Phi}_U(t_0 + T, t_c)\underline{\Phi}_U^{-1}(t_\beta, t_c)\underline{S}_\beta\underline{\Phi}_U(t_\beta, t_c)\underline{\Phi}_U(t_c, t_0)\underline{\Phi}_U^{-1}(t_\alpha, t_0)\underline{S}_\alpha\underline{\Phi}_U(t_\alpha, t_0) \tag{3.35}$$

With the relations

$$\begin{aligned} \underline{\Phi}_U(t_0 + T, t_c)\underline{\Phi}_U^{-1}(t_\beta, t_c) &= \underline{\Phi}_U(t_0 + T, t_c)\underline{\Phi}_U(t_c, t_0)\underline{\Phi}_U^{-1}(t_c, t_0)\underline{\Phi}_U^{-1}(t_\beta, t_c) \\ &= \underline{\Phi}_U(t_0 + T, t_0)\underline{\Phi}_U^{-1}(t_\beta, t_0) \end{aligned} \tag{3.36}$$

and

$$\underline{\Phi}_U(t_\beta, t_c)\underline{\Phi}_U(t_c, t_0) = \underline{\Phi}_U(t_\beta, t_0) \tag{3.37}$$

we obtain

$$\underline{\Phi}(t_0 + T, t_0) = \underline{\Phi}_U(t_0 + T, t_0)\underline{\Phi}_U^{-1}(t_\beta, t_0)\underline{S}_\beta\underline{\Phi}_U(t_\beta, t_0)\underline{\Phi}_U^{-1}(t_\alpha, t_0)\underline{S}_\alpha\underline{\Phi}_U(t_\alpha, t_0) \tag{3.38}$$

which we can rewrite as

$$\underline{\Phi}(t_0 + T, t_0) = \underline{\Phi}_U(t_0 + T, t_0)\underline{C}_\beta(t_\beta, t_0)\underline{C}_\alpha(t_\alpha, t_0) \tag{3.39}$$

Thus

$$\underline{C}(t_0 + T, t_0) = \underline{C}_\beta(t_\beta, t_0)\underline{C}_\alpha(t_\alpha, t_0) \tag{3.40}$$

Let the system possess N discontinuities on the interval $W = \{t \in I\!R \mid 0 \leq t \leq T\}$ and let the discontinuities be located at t_i where $i = 1 \ldots N$. Suppose that we are able to define N associated saltation matrices $\underline{S}_i$. We can now construct a conversion matrix over the period time T

$$\underline{C}(T + t_0, t_0) = \prod_{i=1}^{N} \underline{\Phi}_U^{-1}(t_{N-i+1}, t_0)\underline{S}_{N-i+1}\underline{\Phi}_U(t_{N-i+1}, t_0) \tag{3.41}$$

The conversion matrix maps the unwrapped fundamental solution matrix to the fundamental solution matrix

$$\underline{\Phi}(T + t_0, t_0) = \underline{\Phi}_U(T + t_0, t_0)\underline{C}(T + t_0, t_0) \tag{3.42}$$

3.6 Total procedure for the extended theory of Aizerman and Gantmakher

Suppose we want to obtain the fundamental solution matrix over a period time T which is used in shooting methods to find periodic solutions. The extended method to calculate the fundamental solution matrix is:

1. Integrate the IVP from $t = t_0$ to $t = t_0 + T$

$$\begin{bmatrix} \dot{\underset{\sim}{x}} \\ \dot{\underline{\Phi}}_U \end{bmatrix} = \begin{bmatrix} \underset{\sim}{f}(t, \underset{\sim}{x}) \\ \frac{\partial \underset{\sim}{f}^*}{\partial \underset{\sim}{x}}\ \underline{\Phi}_U \end{bmatrix}, \qquad \underset{\sim}{x}(t_0) = \underset{\sim}{x}_0, \quad \underline{\Phi}_U(t_0, t_0) = \underline{I}. \tag{3.43}$$

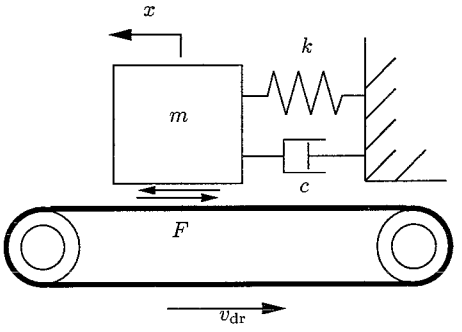

Figure 4.1: 1–DOF model with dry friction

2. From $\underset{\sim}{x}(t)$ find N crossings $\underset{\sim}{x}(t_i)$ with hyper-planes of discontinuities, $i = 1 \ldots N$.

3. Construct the N saltation matrices $\underline{S}_i$ from $\underset{\sim}{x}(t_i)$.

4. Construct the conversion matrix

$$\underline{C}(t_0 + T, t_0) = \prod_{i=1}^{N} \underline{\Phi}_U^{-1}(t_{N-i+1}, t_0)\underline{S}_{N-i+1}\underline{\Phi}_U(t_{N-i+1}, t_0).$$

5. Find the fundamental solution matrix $\underline{\Phi}(t_0 + T, t_0) = \underline{\Phi}_U(t_0 + T, t_0)\underline{C}(t_0 + T, t_0)$.

4 Application of the extended theory of Aizerman and Gantmakher

4.1 Example I: The Stick-slip System

To demonstrate the above theory we will study a one-dimensional system with dry friction that possesses a stick-slip limit cycle.

Consider a mass m attached to inertial space by a spring k and damper c (Figure 4.1). The mass is riding on a driving belt, that is moving at a constant velocity v_{rel}. A friction force F acts between the mass and belt which is dependent on the relative velocity (see Appendix A for the parameter values).

The state equation of this autonomous system reads

$$\dot{\underset{\sim}{x}} = \underset{\sim}{f}(\underset{\sim}{x}) = \begin{bmatrix} \dot{x} \\ -\dfrac{k}{m}x - \dfrac{c}{m}\dot{x} + \dfrac{F}{m} \end{bmatrix}, \tag{4.1}$$

where $\underset{\sim}{x} = [\ x \quad \dot{x}\ ]^T$ and F is given by

$$F(v_{\text{rel}}, x) = \begin{cases} F(v_{\text{rel}}) = -F_{\text{slip}} \operatorname{sgn} v_{\text{rel}}, & v_{\text{rel}} \neq 0 \quad \text{slip} \\ F(x) = \min(|kx + c\dot{x}|, F_{\text{stick}}) \operatorname{sgn}(kx + c\dot{x}), & v_{\text{rel}} = 0 \quad \text{stick} \end{cases} \tag{4.2}$$

The maximum static friction force is denoted by F_{stick} and $v_{\text{rel}} = \dot{x} - v_{\text{dr}}$ is the relative velocity. The constitutive relation for F is the known as the *signum model with static friction point.*

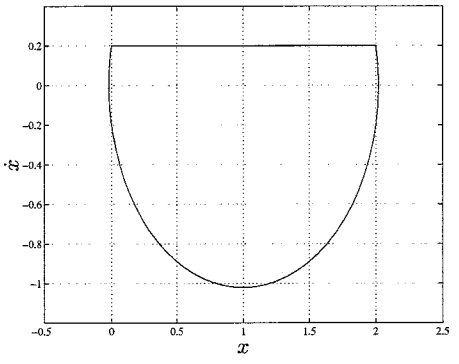

Figure 4.2: Phase portrait

This model permits analytical solutions for $c = 0$ due to its simplicity but it is not directly applicable in numerical analysis. The relative velocity will most likely not be exactly zero in digital computation. Instead, an adjoint *switch model* will be studied which is discontinuous but yields a set of ordinary (and non-stiff!) differential equations. The state equation for the switch model reads

$$\dot{\underset{\sim}{x}} = \begin{cases} \begin{bmatrix} \dot{x} \\ -\frac{k}{m}x - \frac{c}{m}\dot{x} - \frac{F_{\text{slip}}}{m}\operatorname{sgn} v_{\text{rel}} \end{bmatrix} & |v_{\text{rel}}| > \eta \text{ or } |kx + c\dot{x}| > F_{\text{stick}} \\ \begin{bmatrix} v_{\text{dr}} \\ -v_{\text{rel}}\sqrt{\frac{k}{m}} \end{bmatrix} & |v_{\text{rel}}| < \eta \text{ and } |kx + c\dot{x}| < F_{\text{stick}} \end{cases} \tag{4.3}$$

A region of near-zero velocity is defined as $|v_{\text{rel}}| < \eta$ where $\eta \ll v_{\text{dr}}$. Thus, the space R^2 is divided in three subspaces V, W and D as indicated in Figure 4.3. The boundaries between the subspaces are denoted by bold lines. The small parameter η is enlarged to make D visible.

A stable stick-slip limit cycle of this system exists (Figure 4.2). As this system is autonomous, the hyper-surfaces are not dependent on time. It can be seen that the state traverses V (the slip phase) and D (the stick phase). If the state leaves V and enters D, the hyper-surface Σ_α is crossed with normal $\underset{\sim}{n}_\alpha$ where

$$h_\alpha = \dot{x} - v_{\text{dr}}, \tag{4.4}$$

and

$$\underset{\sim}{n}_\alpha = \begin{bmatrix} 0 \\ 1 \end{bmatrix}. \tag{4.5}$$

Likewise, if the state leaves D and enters V again, the hyper-surface Σ_β is crossed with normal $\underset{\sim}{n}_\beta$ where

$$h_\beta = kx + cv_{\text{dr}} - F_{\text{stick}}, \tag{4.6}$$

and

$$\underset{\sim}{n}_\beta = \begin{bmatrix} 1 \\ 0 \end{bmatrix}. \tag{4.7}$$

Let us assume that the state vector crosses Σ_α at $t = t_\alpha$ and Σ_β at $t = t_\beta$. We can now construct the saltation matrices $\underline{S}_\alpha$ and $\underline{S}_\beta$. The right-hand sides at $t = t_\alpha$ for $\lim \eta \downarrow 0$ are

$$\underset{\sim}{f}_{\alpha-} = \begin{bmatrix} v_{\text{dr}} \\ \ddot{x}_{\alpha-} \end{bmatrix}, \qquad \underset{\sim}{f}_{\alpha+} = \begin{bmatrix} v_{\text{dr}} \\ 0 \end{bmatrix}. \tag{4.8}$$

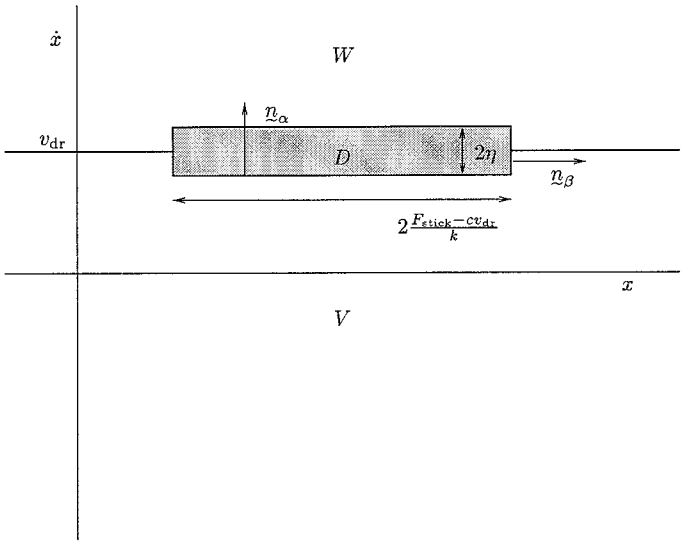

Figure 4.3: Definition of subspaces V, W and D

Thus $\underset{\sim}{S}_\alpha$ yields

$$\underset{\sim}{S}_\alpha = \underline{I} + \frac{(\underset{\sim}{f}_{\alpha+} - \underset{\sim}{f}_{\alpha-})\underset{\sim}{n}_\alpha^T}{\underset{\sim}{n}_\alpha^T \underset{\sim}{f}_{\alpha-}} = \begin{bmatrix} 1 & 0 \\ 0 & 0 \end{bmatrix}, \tag{4.9}$$

which is independent of any system parameter.

Conducting the same for $\underset{\sim}{S}_\beta$ yields

$$\underset{\sim}{f}_{\beta-} = \begin{bmatrix} v_{\mathrm{dr}} \\ 0 \end{bmatrix}, \qquad \underset{\sim}{f}_{\beta+} = \begin{bmatrix} v_{\mathrm{dr}} \\ -\frac{\Delta F}{m} \end{bmatrix}, \tag{4.10}$$

with $\Delta F = F_{\mathrm{stick}} - F_{\mathrm{slip}}$. Substitution yields $\underset{\sim}{S}_\beta$

$$\underset{\sim}{S}_\beta = \underline{I} + \frac{(\underset{\sim}{f}_{\beta+} - \underset{\sim}{f}_{\beta-})\underset{\sim}{n}_\beta^T}{\underset{\sim}{n}_\beta^T \underset{\sim}{f}_{\beta-}} = \begin{bmatrix} 1 & 0 \\ -\frac{\Delta F}{m v_{\mathrm{dr}}} & 1 \end{bmatrix}. \tag{4.11}$$

The solution of the limit cycle only crosses Σ_α and Σ_β once, thus the conversion matrix reads

$$\underline{C}(t_0 + T, t_0) = \underline{\Phi}_U^{-1}(t_\beta, t_0)\underline{S}_\beta \underline{\Phi}_U(t_\beta, t_0)\underline{\Phi}_U^{-1}(t_\alpha, t_0)\underline{S}_\alpha \underline{\Phi}_U(t_\alpha, t_0). \tag{4.12}$$

Note that the saltation matrix $\underline{S}_\alpha$ is singular causing the conversion matrix and fundamental solution matrix to be singular. The physical meaning of this is that the flow of the state vector is uniquely mapped from $\underset{\sim}{x}_0$ to $\underset{\sim}{x}_T$ but the inverse mapping does not exist. If different vector bundles enter the stick phase, they all pass the same states on the stick phase and leave the stick phase from the same state $\underset{\sim}{x}_\beta$. So, if the flow enters the stick phase, knowledge about its initial state is lost. The fundamental solution matrix for the limit cycle of system Equation 4.3 is plotted in Figure 4.4. Jumps at $t = t_\alpha$ and $t = t_\beta$ in the fundamental solution matrix can be distinguished. The continuous unwrapped fundamental solution matrix is plotted in Figure 4.5. The time derivative clearly changes at $t = t_\alpha$ and $t = t_\beta$ but the components of $\underline{\Phi}_U$ remain continuous.

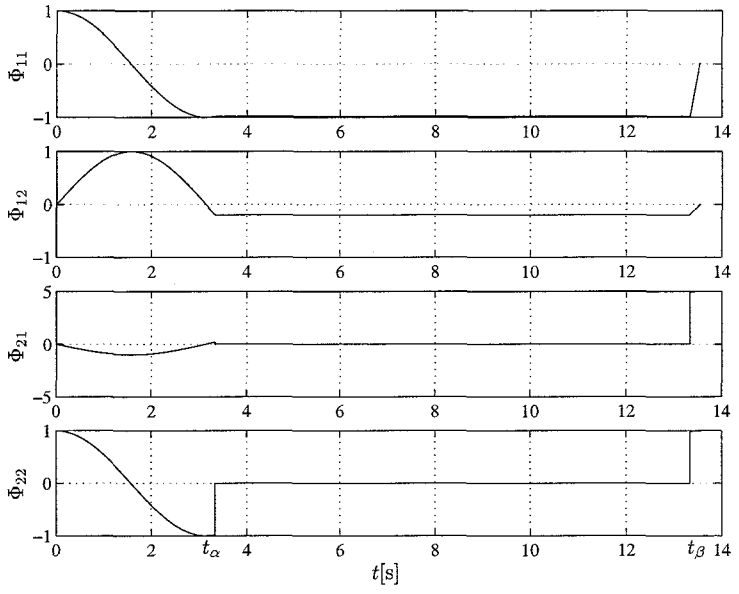

Figure 4.4: Fundamental solution matrix

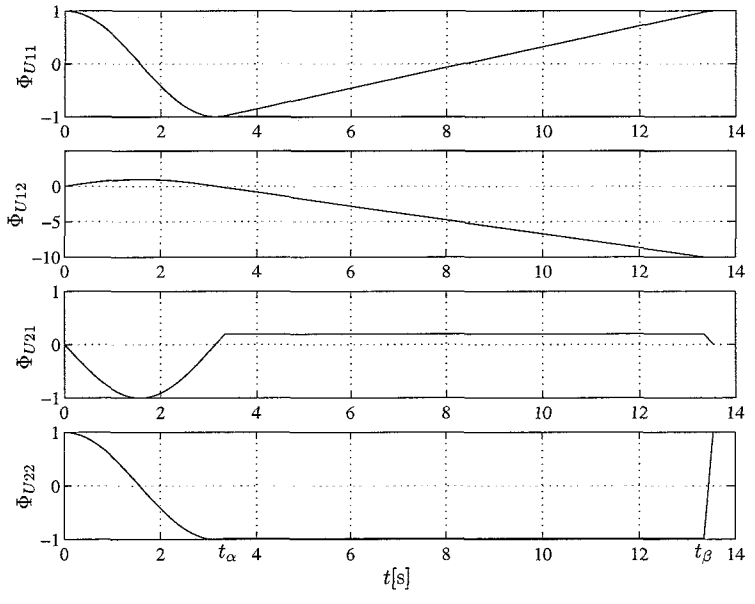

Figure 4.5: Unwrapped fundamental solution matrix

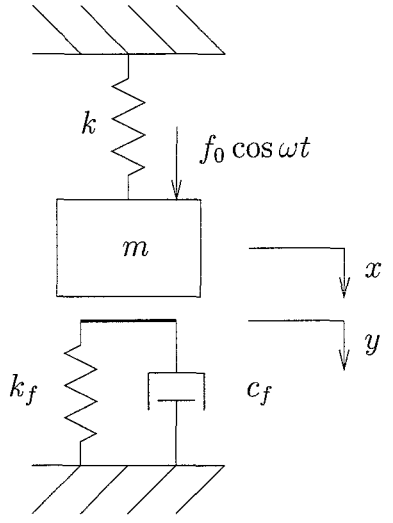

Figure 4.6: Mass with discontinuous support

4.2 Example II: The Discontinuous Support

As a second example we will consider a mass-spring system with a discontinuous support (Figure 4.6). The support is massless, has a spring stiffness k_f and damping coefficient c_f, which makes the support a first-order system. The state vector is chosen to be $\underset{\sim}{x} = \begin{bmatrix} x & \dot{x} & y \end{bmatrix}^{\mathrm{T}}$. The system has two possible states: the mass is in contact with the support or the mass is not in contact with the support. Let f_c denote the contact force between mass and support. If the mass is not in contact the following holds:

$$x < y \quad \text{and} \quad f_c = 0,$$

and if the mass is in contact:

$$x = y \quad \text{and} \quad f_c = k_f y + c_f \dot{y} \geq 0.$$

The hyper-surface Σ divides the state space in the subspaces

$$V_- = \{x, y \in I\!R^2 \mid x - y < 0, k_f y + c_f \dot{y} = 0\} \quad \text{(no contact)}$$

and

$$V_+ = \{x, y \in I\!R^2 \mid x - y = 0, k_f y + c_f \dot{y} \geq 0\} \quad \text{(contact)}.$$

Thus the hyper-surface Σ consist of the conjunction of two surfaces Σ_α and Σ_β. The hyper-surface Σ_α is defined by the indicator function

$$h_\alpha = x - y = 0 \tag{4.13}$$

but is limited to $k_f y + c_f \dot{y} = 0$. The surface Σ_α has the normal

$$\underset{\sim}{n}_\alpha = \begin{bmatrix} 1 \\ 0 \\ -1 \end{bmatrix}. \tag{4.14}$$

The hyper-surface Σ_β is defined by the indicator function

$$h_\beta = k_f y + c_f \dot{y} = 0, \tag{4.15}$$

but is limited to $x - y = 0$. Thus the indicator function h_β can be replaced by

$$h_\beta = k_f x + c_f \dot{x} = 0. \tag{4.16}$$

The surface Σ_β has the normal

$$\underset{\sim}{n}_\beta = \begin{bmatrix} k_f \\ c_f \\ 0 \end{bmatrix}. \tag{4.17}$$

The state equation of this non-autonomous system reads

$$\dot{\underset{\sim}{x}}(t) = \underset{\sim}{f}(t, \underset{\sim}{x}(t)) = \begin{cases} \underset{\sim}{f}_-(t, \underset{\sim}{x}(t)) & \underset{\sim}{x} \in V_- \\ \underset{\sim}{f}_+(t, \underset{\sim}{x}(t)) & \underset{\sim}{x} \in V_+, \end{cases} \tag{4.18}$$

with

$$\underset{\sim}{f}_-(t, \underset{\sim}{x}) = \begin{bmatrix} \dot{x} \\ -\frac{k}{m}x + \frac{f_0}{m}\cos\omega t \\ -\frac{k_f}{c_f}y \end{bmatrix}, \tag{4.19}$$

and

$$\underset{\sim}{f}_+(t, \underset{\sim}{x}) = \begin{bmatrix} \dot{x} \\ -\frac{k+k_f}{m}x - \frac{c_f}{m}\dot{x} + \frac{f_0}{m}\cos\omega t \\ \dot{x} \end{bmatrix}. \tag{4.20}$$

We first consider the transition from the state without contact to the state with contact. Let us assume that the state vector crosses Σ, leaving V_- and entering V_+, at $t = t_\alpha$. The state thus crosses the Σ_α part of Σ at this instance. We can now construct the saltation matrix $\underline{S}_\alpha$. The right-hand sides at the instance t_α are

$$\underset{\sim}{f}_{\alpha-} = \begin{bmatrix} \dot{x}_\alpha \\ -\frac{k}{m}x_\alpha + \frac{f_0}{m}\cos\omega t_\alpha \\ -\frac{k_f}{c_f}x_\alpha \end{bmatrix}, \tag{4.21}$$

$$\underset{\sim}{f}_{\alpha+} = \begin{bmatrix} \dot{x}_\alpha \\ -\frac{k+k_f}{m}x_\alpha - \frac{c_f}{m}\dot{x}_\alpha + \frac{f_0}{m}\cos\omega t_\alpha \\ \dot{x}_\alpha \end{bmatrix}. \tag{4.22}$$

Thus $\underline{S}_\alpha$ yields

$$\begin{aligned} \underline{S}_\alpha &= \underline{I} + \frac{(\underset{\sim}{f}_{\alpha+} - \underset{\sim}{f}_{\alpha-})\underset{\sim}{n}_\alpha^T}{\underset{\sim}{n}_\alpha^T \underset{\sim}{f}_{\alpha-}} \\ &= \underline{I} + \begin{bmatrix} 0 & 0 & 0 \\ -\frac{c_f}{m} & 0 & \frac{c_f}{m} \\ 1 & 0 & -1 \end{bmatrix} = \begin{bmatrix} 1 & 0 & 0 \\ -\frac{c_f}{m} & 1 & \frac{c_f}{m} \\ 1 & 0 & 0 \end{bmatrix}. \end{aligned} \tag{4.23}$$

We now consider the transition from the state with contact to the state without contact. Let us assume that the state vector crosses Σ, leaving V_+ and entering V_-, at $t = t_\beta$. The state thus crosses the Σ_β part of Σ at this instance. Consequently, the following holds

$$x_\beta = y_\beta, \tag{4.24}$$

and

$$k_f x_\beta + c_f \dot{x}_\beta = 0. \tag{4.25}$$

We can now construct the saltation matrix $\underline{S}_\beta$. The right-hand sides at the instance t_β are

$$\underset{\sim}{f}_{\beta-} = \begin{bmatrix} \dot{x}_\beta \\ -\frac{k+k_f}{m}x_\beta - \frac{c_f}{m}\dot{x}_\beta + \frac{f_0}{m}\cos\omega t_\beta \\ \dot{x}_\beta \end{bmatrix}, \tag{4.26}$$

$$\underset{\sim}{f}_{\beta+} = \begin{bmatrix} \dot{x}_\beta \\ -\frac{k}{m}x_\beta + \frac{f_0}{m}\cos\omega t_\beta \\ -\frac{k_f}{c_f}y_\beta \end{bmatrix}. \tag{4.27}$$

If we substitute Equations 4.24 and 4.25 in Equations 4.26 and Equation 4.27, then the latter equations appear to be identical

$$\underset{\sim}{f}_{\beta-} = \underset{\sim}{f}_{\beta+}.$$

Thus $\underline{S}_\beta$ is just the identity matrix.

$$\underline{S}_\beta = \underline{I} \tag{4.28}$$

The results show that the saltation matrices $\underline{S}_\alpha$ and $\underline{S}_\beta$ are not dependent on the support stiffness k_f. The saltation matrix $\underline{S}_\alpha$ is affected, however, by the ratio $\frac{c_f}{m}$. The physical interpretation must be sought in the discontinuity of the contact force f_c. The spring force will be equal before and after the transition, as the displacements x and y are continuous in time. But the damping force, induced by the dashpot, will not be equal before and after the transition, as the velocity $\dot{y}$ is discontinuous at the transition from no-contact to contact. For the transition from contact to no-contact, the velocity $\dot{y}$ is continuous which is the reason that $\underline{S}_\beta$ is equal to the identity matrix.

If the damping coefficient c_f is set to zero, the system reduces to a second order system with discontinuous stiffness. In this case, the hyper-surfaces Σ_α and Σ_β are identical and the saltation matrices $\underline{S}_\alpha$ and $\underline{S}_\beta$ are both equal to the identity matrix. It can be concluded that the jumps in the fundamental solution matrix are not caused by the discontinuous stiffness but by the discontinuous damping term.

5 Linear Approximations at the Discontinuity

5.1 Introduction

Discontinuities in the vector field $\underset{\sim}{f}$ cause jumps in the fundamental solution matrix as was shown in the preceding section. The discontinuous differential equation is therefore often approximated by a continuous differential equation. The approximation can be chosen to be smooth, which is called the *smoothing method*, but this is not necessary. The approximation should at least yield a continuous differential equation and be asymptotic.

We employ a special approximation in the sequel for analytical purposes. The jump of the vector field $\underset{\sim}{f}$ is approximated by a linear variation of $\underset{\sim}{f}$ from $\underset{\sim}{f}_-$ to $\underset{\sim}{f}_+$ in a thin space around the hyperplane of discontinuity.

It will be shown that this linear approximation of the vector field at the hyperplane of discontinuity also yields a linear variation of the saltation matrix.

The linear approximation at the discontinuity is suitable for analytical purposes, due to its simplicity, and will prove to be an important tool in the bifurcation analysis of discontinuous systems.

5.2 A single hyperplane

Consider again the discontinuous system 3.1 where the indicator equation h defines the hypersurface of discontinuity Σ.

$$\dot{\underset{\sim}{x}}(t) = \underset{\sim}{f}(t, \underset{\sim}{x}(t); \mu) = \begin{cases} \underset{\sim}{f}_-(t, \underset{\sim}{x}(t); \mu) & (\underset{\sim}{x}, \mu) \in V_- \\ \underset{\sim}{f}_-(t, \underset{\sim}{x}(t); \mu) & (\underset{\sim}{x}, \mu) \in \Sigma \\ \underset{\sim}{f}_+(t, \underset{\sim}{x}(t); \mu) & (\underset{\sim}{x}, \mu) \in V_+, \end{cases} \tag{5.1}$$

with

$$\begin{aligned} V_- &= \{(\underset{\sim}{x}, \mu) \in I\!R^{n+1} \mid h(t, \underset{\sim}{x}(t); \mu) < 0\} \\ \Sigma &= \{(\underset{\sim}{x}, \mu) \in I\!R^{n+1} \mid h(t, \underset{\sim}{x}(t); \mu) = 0\} \\ V_+ &= \{(\underset{\sim}{x}, \mu) \in I\!R^{n+1} \mid h(t, \underset{\sim}{x}(t); \mu) > 0\} \end{aligned} \tag{5.2}$$

where the vector field $\underset{\sim}{f}$ and the indicator function h are also functions of a scalar control parameter μ. In the following we will briefly denote a function $\underset{\sim}{g}(t, \underset{\sim}{x}(t); \mu)$ by $\underset{\sim}{g}$.

The hyperplane Σ will now be replaced by a thin space $\tilde{\Sigma}$ with thickness ε. If ε approaches zero, then the space $\tilde{\Sigma}$ becomes infinitely thin. The vector field in $\tilde{\Sigma}$ varies linearly from $\underset{\sim}{f}_-$ to $\underset{\sim}{f}_+$.

$$\dot{\underset{\sim}{x}}(t) = \underset{\sim}{\tilde{f}} = \begin{cases} \underset{\sim}{f}_- & (\underset{\sim}{x}, \mu) \in \tilde{V}_- \\ (\underset{\sim}{f}_+ - \underset{\sim}{f}_-)\frac{h}{\varepsilon} + \underset{\sim}{f}_- & (\underset{\sim}{x}, \mu) \in \tilde{\Sigma} \\ \underset{\sim}{f}_+ & (\underset{\sim}{x}, \mu) \in \tilde{V}_+, \end{cases} \tag{5.3}$$

with

$$\begin{aligned} \tilde{V}_- &= \{(\underset{\sim}{x}, \mu) \in I\!R^{n+1} \mid h(t, \underset{\sim}{x}(t)) < 0\} \\ \tilde{\Sigma} &= \{(\underset{\sim}{x}, \mu) \in I\!R^{n+1} \mid 0 \leq h(t, \underset{\sim}{x}(t)) \leq \varepsilon\} \\ \tilde{V}_+ &= \{(\underset{\sim}{x}, \mu) \in I\!R^{n+1} \mid h(t, \underset{\sim}{x}(t)) > \varepsilon\} \end{aligned} \tag{5.4}$$

The vector field $\underset{\sim}{\tilde{f}}$ is thus continuous and converges asymptotically to $\underset{\sim}{f}$ as $\varepsilon \downarrow 0$. The Jacobian of $\underset{\sim}{\tilde{f}}$ follows from Equation 5.3 to be

$$\underline{\tilde{J}} = \begin{cases} \underline{J}_- & (\underset{\sim}{x}, \mu) \in \tilde{V}_- \\ (\underset{\sim}{f}_+ - \underset{\sim}{f}_-)\frac{n^T}{\varepsilon} + (\underline{J}_+ - \underline{J}_-)\frac{h}{\varepsilon} + \underline{J}_- & (\underset{\sim}{x}, \mu) \in \tilde{\Sigma} \\ \underline{J}_+ & (\underset{\sim}{x}, \mu) \in \tilde{V}_+, \end{cases} \tag{5.5}$$

and is in fact not properly defined on the borders between $\tilde{V}_-$,$\tilde{V}_+$ and $\tilde{\Sigma}$ as $\underset{\sim}{\tilde{f}}$ is not necessarily smooth. This will turn out to be not problematic.

We are interested in bifurcations of periodic solutions of discontinuous systems. The fundamental solution matrix of a discontinuous system can jump as we elaborated in Section 3. A periodic solution can be envisaged a fixed point of a Poincaré map P on a Poincaré section. The derivative of the Poincaré map DP can therefore also jump as it is directly related to the fundamental solution matrix. The Poincaré map itself is continuous. As periodic solutions are fixed points of P we will also study bifurcations of fixed points of non-smooth systems. Having periodic solutions in mind we will study only fixed points of continuous vector fields with discontinuous Jacobians. Thus we consider continuous but non-smooth *mappings*:

Bifurcations of fixed points: the vector field is
- a) continuous: $\underset{\sim}{f}_- = \underset{\sim}{f}_+$ if $\underset{\sim}{x}(t) \in \Sigma$
- b) non-smooth: $\underline{J}_- \neq \underline{J}_+$ if $\underset{\sim}{x}(t) \in \Sigma$

Bifurcations of periodic solutions: the Poincaré map is

a) continuous: $P_- = P_+$

b) non-smooth: $DP_- \neq DP_+$, which yields $\underset{\sim}{f}_- \neq \underset{\sim}{f}_+$ if $(\underset{\sim}{x}(t), \mu) \in \Sigma$

Remarks. The statement that only continuous mappings will be considered is too restrictive. Poincaré mappings are in general discontinuous (for example the Lorenz system [8] page 313). We will mainly consider mappings which are continuous in a sufficiently large neighborhoud around the fixed point of the mapping. In Section 7.8, however, an example will be given where the Poincaré map is discontinuous at the fixed point, which results in infinitely unstable periodic solutions. Note that this is a sliding mode problem for which Equation 3.5 does not hold.

We now study how the saltation matrix changes as the flow is crossing the space $\tilde{\Sigma}$. We denote the state at the border of $\underset{\sim}{V}_-$ and $\tilde{\Sigma}$ by $\underset{\sim}{x}_0$ at time t_0. Let the flow travel starting from $\underset{\sim}{x}_0$ a distance $\Delta\underset{\sim}{x}$ in $\tilde{\Sigma}$ during a time Δt.

We expand the indicator function h as a Taylor approximation around $\underset{\sim}{x}_0$ for fixed μ and assume an autonomous h for simplicity.

$$h(\underset{\sim}{x}_0 + \Delta\underset{\sim}{x}) = h(\underset{\sim}{x}_0) + \frac{\partial h}{\partial \underset{\sim}{x}^T}\Delta\underset{\sim}{x} + O(\Delta\underset{\sim}{x}^2) \tag{5.6}$$

As ε approaches zero, the space $\tilde{\Sigma}$ becomes infinitely thin and $\Delta\underset{\sim}{x} \downarrow \underset{\sim}{0}$ and $\Delta t \downarrow 0$. It therefore suffices to take only the linear term into account in the Taylor approximation of Equation 5.6 as $\varepsilon \downarrow 0$. It follows from the definition of $\tilde{V}_-$ in Equation 5.4 that

$$h(\underset{\sim}{x}_0) = 0 \tag{5.7}$$

and that

$$0 \leq h(\underset{\sim}{x}_0 + \Delta\underset{\sim}{x}) \leq \varepsilon. \tag{5.8}$$

Consequently, it is allowed to express the indicator function for $\varepsilon \downarrow 0$ as a linear function of a variable q

$$h(q) = q\varepsilon \tag{5.9}$$

where $0 \leq q \leq 1$. The variable q is a variable over the space $\tilde{\Sigma}$, where $q = 0$ corresponds to the border between $\tilde{V}_-$ and $\tilde{\Sigma}$ and $q = 1$ corresponds to the border between $\tilde{\Sigma}$ and $\tilde{V}_+$.

Similarly, we express the distance $\Delta\underset{\sim}{x}$ as a Taylor approximation up to the linear term with $\Delta t \downarrow 0$ for $\varepsilon \downarrow 0$

$$\Delta\underset{\sim}{x} = \int_{t_0}^{t_0+\Delta t} \underset{\sim}{\tilde{f}} dt = \underset{\sim}{f}_- \Delta t + O(\Delta t^2) \tag{5.10}$$

Substitution of Equation 5.7 and 5.9 in Equation 5.6 yields

$$q\varepsilon = \underset{\sim}{n}^T \underset{\sim}{f}_- \Delta t \tag{5.11}$$

for $\varepsilon \downarrow 0$.

The Jacobian can be approximated for small ε and bounded $\underset{\sim}{\tilde{f}}$ by

$$\underline{\tilde{J}} = \frac{1}{\varepsilon}(\underset{\sim}{f}_+ - \underset{\sim}{f}_-)\underset{\sim}{n}^T + O(1) \tag{5.12}$$

which becomes *large* for $\varepsilon \downarrow 0$. We can now construct the saltation matrix $\underline{\tilde{S}} = \underline{\Phi}(\Delta t, 0)$ for $\varepsilon \downarrow 0$ from the previous results

$$\begin{aligned} \underline{\tilde{S}} &= \underline{I} + \int_0^{\Delta t} \underline{\tilde{J}}\,\underline{\Phi} dt \\ &= \underline{I} + (\underset{\sim}{f}_+ - \underset{\sim}{f}_-)\frac{\underset{\sim}{n}^T}{\varepsilon}\Delta t + O(\Delta t) \\ &= \underline{I} + q\frac{(\underset{\sim}{f}_+ - \underset{\sim}{f}_-)\underset{\sim}{n}^T}{\underset{\sim}{n}^T \underset{\sim}{f}_-} + O(\Delta t) \end{aligned} \tag{5.13}$$

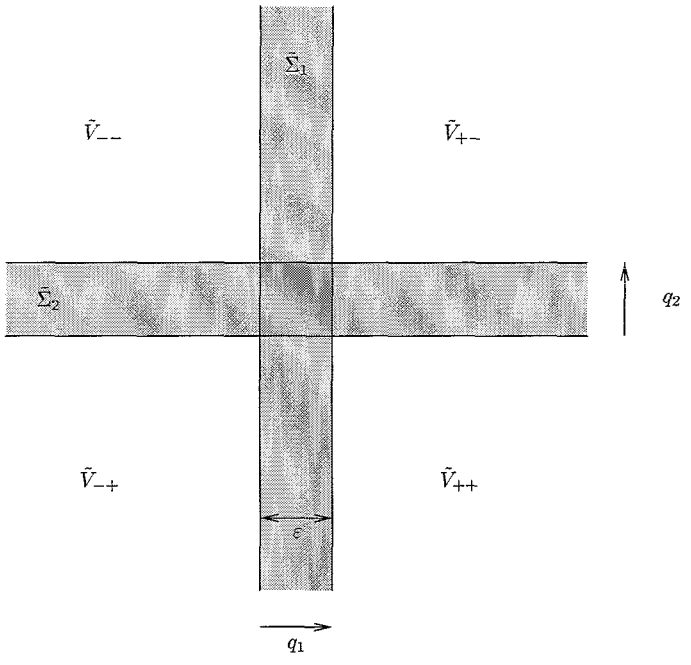

Figure 5.1: Linear approximation with two hyperplanes

Thus the saltation matrix $\underset{\sim}{\tilde{S}}$ converges to

$$\begin{aligned} \underset{\sim}{\tilde{S}} &= \underline{I} + q\frac{(\underset{\sim}{f}_+ - \underset{\sim}{f}_-)\underset{\sim}{n}^T}{\underset{\sim}{n}^T\underset{\sim}{f}_-} \\ &= \underline{I} + q(\underline{S} - \underline{I}) \end{aligned} \tag{5.14}$$

where $\underline{S}$ is the saltation matrix over Σ given by Equation 3.25. The saltation matrix thus behaves linearly over $\tilde{\Sigma}$ if $\varepsilon \downarrow 0$. The derivation is given for autonomous h but the same result could have been obtained for non-autonomous h.

For fixed points we have $\underset{\sim}{f}_- = \underset{\sim}{f}_+$ and the Jacobian is thus given by

$$\underline{\tilde{J}}(q) = (\underline{J}_+ - \underline{J}_-)q + \underline{J}_-, (\underset{\sim}{x}, \mu) \in \tilde{\Sigma} \tag{5.15}$$

The Jacobian of fixed points behaves thus linearly in $\tilde{\Sigma}$. For fixed points, the linear approximation smoothes the continuous non-smooth vector field. For periodic solutions, the linear approximation replaces the discontinuous vector field by a continuous vector field.

5.3 A double hyperplane

The fixed point could also be located on the intersection of two hyperplanes Σ_1 and Σ_2. The linear approximation is analogous to the one given in the previous section but more elaborate. Each hyperplane Σ_j has now to be replaced by a corresponding thin space $\tilde{\Sigma}_j$ with parameter q_j (Figure 5.1). The fixed point is located in the double hatched zone where the hyperplanes intersect. The two hyperplanes divide the state-space in four spaces V_{--}, V_{+-}, V_{-+} and V_{++} with Jacobians $\underline{J}_{--}$, $\underline{J}_{+-}$, $\underline{J}_{-+}$ and $\underline{J}_{++}$. The linear approximation of the Jacobian over hyperplane $\tilde{\Sigma}_1$ at the fixed point is

$$\begin{aligned} \underline{\tilde{J}}_I &= q_1(\underline{J}_{+-} - \underline{J}_{--}) + \underline{J}_{--} \quad \text{above } \tilde{\Sigma}_2 \\ \underline{\tilde{J}}_{II} &= q_1(\underline{J}_{++} - \underline{J}_{-+}) + \underline{J}_{-+} \quad \text{below } \tilde{\Sigma}_2 \end{aligned} \tag{5.16}$$

with

$$\underset{\sim}{J}_{+-} - \underset{\sim}{J}_{--} = \underset{\sim}{J}_{++} - \underset{\sim}{J}_{-+}$$

because the same hyperplane is crossed. With a second linear approximation we can set up the Jacobian over the other hyperplane

$$\begin{aligned} \tilde{\underset{\sim}{J}} &= q_2(\tilde{\underset{\sim}{J}}_{II} - \tilde{\underset{\sim}{J}}_{I}) + \tilde{\underset{\sim}{J}}_{I} \\ &= q_2(\underset{\sim}{J}_{-+} - \underset{\sim}{J}_{--}) + q_1(\underset{\sim}{J}_{+-} - \underset{\sim}{J}_{--}) + \underset{\sim}{J}_{--} \end{aligned} \tag{5.17}$$

which is a linear combination in q_1 and q_2 in the double hatched space around the fixed point.

6 Bifurcations of Fixed Points

6.1 Introduction

In this section we study the bifurcations of fixed points of autonomous first-order systems which are non-smooth and continuous ($\underset{\sim}{f} \in C^0$) and have one control parameter μ:

$$\dot{\underset{\sim}{x}} = \underset{\sim}{f}(\underset{\sim}{x}; \mu). \tag{6.1}$$

Let n denote the dimension of the system 6.1.

This section is to a large extend analogous to the treatment of bifurcations of fixed points for smooth systems in Nayfeh & Balachandran [18].

Fixed points of smooth systems can loose stability through one of the following bifurcations: (a) saddle-node bifurcation, (b) transcritical bifurcation, (c) pitchfork bifurcation or (d) Hopf bifurcation. Bifurcations (a)-(c) are static bifurcations and (d) is a dynamic bifurcation of a fixed point. The Jacobian matrices of smooth systems are continuous functions of the state vector and bifurcation parameter. The bifurcations occuring in smooth systems are therefore *continuous bifurcations*. Non-smooth systems possess set-valued Jacobian matrices, which can be treated with linear approximation theory as presented in the preceding section. If the Jacobian matrix at the bifurcation point is set-valued, then the bifurcation is discontinuous. Non-smooth systems can thus lead to continuous bifurcations and to *discontinuous bifurcations* of fixed points. For each of the continuous bifurcations (a)-(d) we try to find a similar discontinuous bifurcation occurring in a non-smooth continuous system. The non-smooth system should be as simple as possible and will therefore be chosen as a piecewise linear continuous function. Thus, the non-smooth system approximates the nonlinear smooth system by a piecewise linear function, thereby preserving the nature of the bifurcation. Note that we are conducting here the opposite of smoothing: we try to find a non-smooth function that has a similar bifurcation diagram. For example, a nonlinear term x^2 of the smooth system can be replaced by a piecewise linear term $|x|$ which is continuous.

The point $(\underset{\sim}{x}^*, \mu^*)$ will denote a bifurcation point in the sequel. The bifurcation point $(\underset{\sim}{x}^*, \mu^*)$ can be located on a hyperplane (or the intersection of hyperplanes) where the vector field is non-smooth. Let b denote the number of hyperplanes going through the bifurcation point. At the bifurcation point we can construct a linear approximation $\tilde{\underset{\sim}{J}}$ for the Jacobian (in the sense of the previous section) with b linear approximation parameters q_j where $j = 1..b$. Let $\underset{\sim}{f}_{,\mu}$ be the partial derivative $\partial \underset{\sim}{f} / \partial \mu$. If $\underset{\sim}{f}_{,\mu}$ is discontinuous at the bifurcation point then it can be approximated by a linear approximation $\tilde{\underset{\sim}{f}}_{,\mu}$.

The linear approximation of the Jacobian $\tilde{\underset{\sim}{J}}(q_j)$ has n eigenvalues $\tilde{\lambda}_i$, where $i = 1, .., n$ which are of course dependent on q_j. We will mostly treat one-dimensional systems in the sequel, thus $n = 1$ and the subscript i will be omitted.

Theorem 1 (Static Bifurcation Theorem)
A static bifurcation of a fixed point of $\dot{\underset{\sim}{x}} = \underset{\sim}{f}(\underset{\sim}{x}; \mu)$ occurs in the $\underset{\sim}{x}$–μ state-control space at $(\underset{\sim}{x}^*, \mu^*)$ if the following two conditions are satisfied:

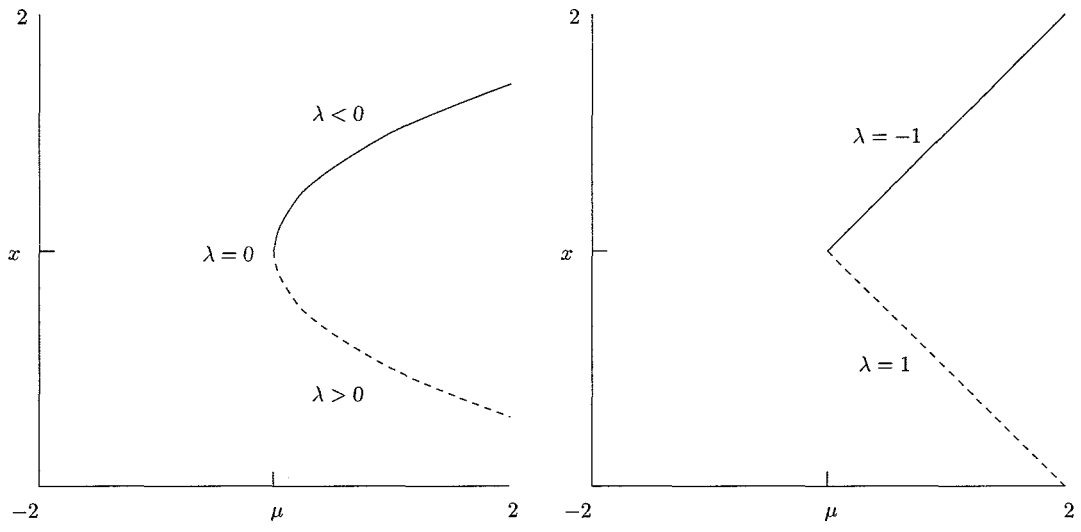

(a) smooth (b) discontinuous

Figure 6.1: Saddle node bifurcation

1. $\underset{\sim}{f}(\underset{\sim}{x}^*, \mu^*) = 0$,
2. $det(\tilde{\underline{J}}(q_j)) = 0$ *for some set* q_j, *where* $0 \leq q_j \leq 1$.

Remarks. The first condition ensures that the solution is a fixed point. The second condition implies that $\tilde{\underline{J}}$ at a fixed point has at least one eigenvalue $\tilde{\lambda}_i = 0$.

First the continuous bifurcation is briefly treated, and then its discontinuous counterpart is discussed. The insight in discontinuous bifurcations of fixed points of non-smooth continuous systems will be of value for the understanding of bifurcations of periodic solutions of discontinuous systems in the next section.

6.2 Saddle-node bifurcation

The smooth scalar system

$$\dot{x} = f(x;\mu) = \mu - x^2 \tag{6.2}$$

has two fixed points for $\mu > 0$

$$x = \sqrt{\mu}, \quad x = -\sqrt{\mu} \ .$$

The Jacobian $\underline{J} = -2x$ becomes singular at $x = 0$, thus there is a bifurcation at $(x, \mu) = (0, 0)$ in the $x - \mu$ space (Figure 6.1a) which is known as a saddle-node bifurcation point. The upper branch is stable (solid line) and the lower one unstable (dashed line). At a continuous saddle-node bifurcation, $f_{,\mu}$ does not belong to the range of the matrix $\underline{J}$. Hence the matrix $[\underline{J}|f_{,\mu}]$ has rank n. This can be geometrically interpreted as stating that the continuation problem is unique. We can follow the branch up to the bifurcation and continue uniquely on the other part of the branch.

We now replace the term x^2 by $|x|$ which yields a non-smooth system:

$$\dot{x} = f(x;\mu) = \mu - |x| \tag{6.3}$$

which has again two fixed points for $\mu > 0$

$$x = \mu, \quad x = -\mu \ .$$

with Jacobian $\underline{J}(x) = -\operatorname{sgn} x$. The linear approximation of the Jacobian $\tilde{\underline{J}}$ at $x = 0$ takes the form

$$\tilde{\underline{J}} = -2q + 1 \tag{6.4}$$

which becomes singular at $q = \frac{1}{2}$. A static bifurcation thus exists at $(x, \mu) = (0, 0)$. Furthermore, $f_{,\mu} = 1$, hence the matrix $\left[\tilde{\underline{J}} | f_{,\mu}\right]$ has rank n at $q = \frac{1}{2}$. The bifurcation scenario is depicted in Figure 6.1b and looks similar to the one for the continuous version. Again there is a stable branch and an unstable branch but they now meet at an acute angle. The jump of the eigenvalue and the acute conjunction of branches are properties of discontinuous bifurcations which we will also encounter for bifurcations of periodic solutions.

Theorem 2 (Saddle-node Bifurcation Theorem)
A saddle-node bifurcation of a fixed point of $\dot{\underset{\sim}{x}} = \underset{\sim}{f}(\underset{\sim}{x}; \mu)$ *occurs in the* $\underset{\sim}{x}$–μ *state-control space at* $(\underset{\sim}{x}^*, \mu^*)$ *if the following conditions are satisfied:*

1. $\underset{\sim}{f}(\underset{\sim}{x}^*, \mu^*) = 0$,
2. $det(\tilde{\underline{J}}(q_j)) = 0$ *for some set* q_j, *where* $0 \leq q_j \leq 1$,
3. $\left[\tilde{\underline{J}} | \underset{\sim}{f}_{,\mu}\right]$ *has rank* n

It should be noted that, if we smooth the non-smooth system with an arctangent for example,

$$\dot{x} = \mu - \frac{2}{\pi} \arctan(\varepsilon x) x = \mu - \frac{2}{\pi} \varepsilon x^2 + O(x^4),$$

the resulting bifurcation will be a continuous saddle-node bifurcation for all ε as can be seen from the expansion around the bifurcation point ($x = 0$). The bifurcation in Figure 6.1b is therefore a discontinuous saddle-node bifurcation.

6.3 Transcritical bifurcation

First, we consider the scalar smooth system

$$\dot{x} = f(x; \mu) = \mu x - x^2 \tag{6.5}$$

There are two fixed points

$$x = 0, \quad x = \mu$$

The Jacobian

$$\underline{J}(x) = \mu - 2x$$

has the single eigenvalue

$$\begin{aligned} \lambda &= \mu, \quad \text{at } x = 0 \\ \lambda &= -\mu, \quad \text{at } x = \mu \end{aligned}$$

The static bifurcation, shown in Figure 6.2a, is a transcritical bifurcation point at which two branches exchange stability. The function $f(x; \mu)$ is depicted in Figure 6.2b for $\mu = -1$, $\mu = 0$ and $\mu = 1$. The function has two distinct zeros for $\mu \neq 0$, where one is always in the origin. At the bifurcation point ($\mu = 0$), the two zeros coincide to one double zero. The two zeros exchange stability when the bifurcation point is passed. At a continuous transcritical bifurcation point, $f_{,\mu}$ does belong to the range of the matrix $\underline{J}$. Hence the matrix $[\underline{J} | f_{,\mu}]$ has rank $n - 1$. A second branch thus crosses the bifurcation point which makes the continuation problem non-unique.

We replace the smooth system 6.5 by the following non-smooth system:

$$\dot{x} = f(x; \mu) = |\frac{1}{2}\mu| - |x - \frac{1}{2}\mu| \tag{6.6}$$

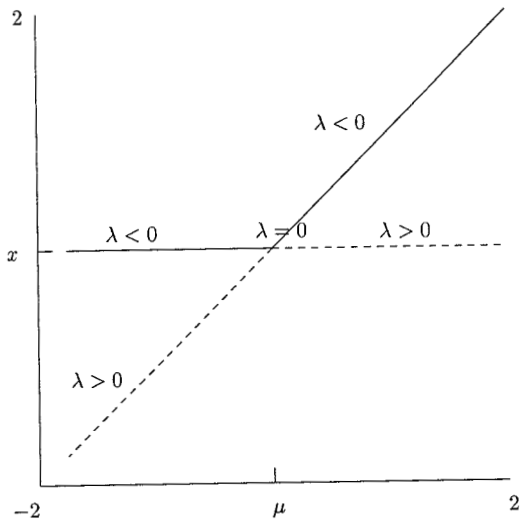

(a) bifurcation diagram

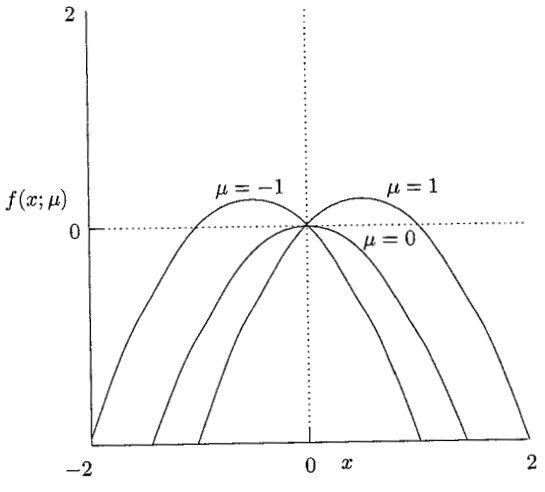

(b) $f(x;\mu)$

Figure 6.2: Transcritical bifurcation, smooth

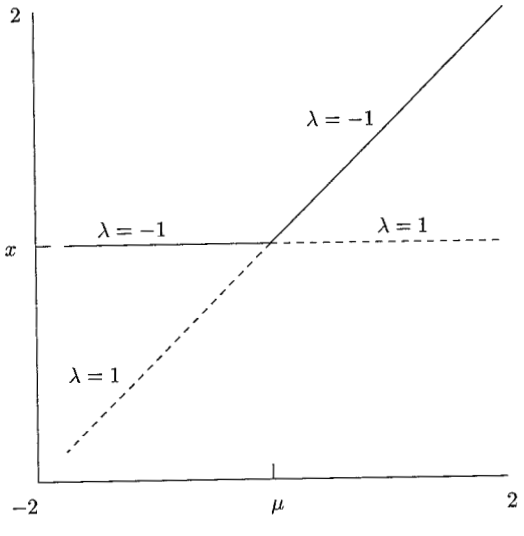

(a) bifurcation diagram

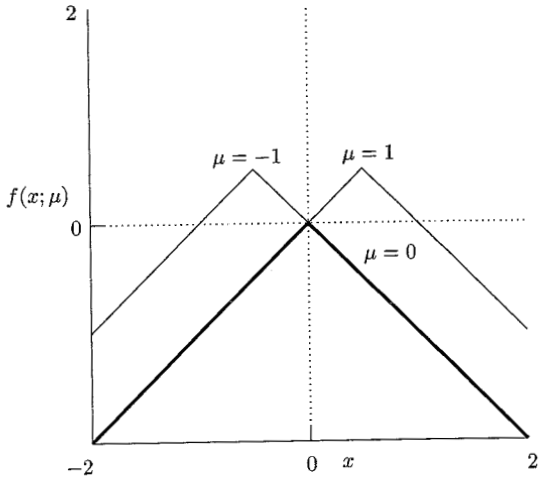

(b) $f(x;\mu)$

Figure 6.3: Transcritical bifurcation, discontinuous

This non-smooth system approximates the parabola in Figure 6.2b by a piecewise linear curve (a tent) as is depicted in Figure 6.3b. The lines are bold where the curves overlap each other. The non-smooth system has the same fixed points as the smooth system

$$x = 0, \quad x = \mu$$

The Jacobian is again discontinuous

$$\underset{\sim}{J}(x) = -\operatorname{sgn}(x - \frac{1}{2}\mu)$$

and is not single valued at $(x, \mu) = (0, 0)$. The Jacobian has the eigenvalues

$$\begin{array}{ll} \lambda = -1, & \text{at } x = 0 \text{ if } \mu < 0 \\ \lambda = 1, & \text{at } x = 0 \text{ if } \mu > 0 \\ \lambda = 1, & \text{at } x = \mu \text{ if } \mu < 0 \\ \lambda = -1, & \text{at } x = \mu \text{ if } \mu > 0 \end{array}$$

The fixed point $(x, \mu) = (0, 0)$ is located on the intersection of two hyperplanes $\mu = 0$ and $x - \frac{1}{2}\mu = 0$ in the (x, μ) space. Two parameters, q_1 and q_2, are needed for a linear approximation. The first parameter, $q - 1$, will be varied to satisfy the condition $det(\tilde{\underset{\sim}{J}}) = 0$ and the second parameter, q_2, will be varied to assure that $\left[\tilde{\underset{\sim}{J}} | \tilde{\underset{\sim}{f}}_{,\mu}\right]$ has rank $n - 1$.

The linear approximation $\tilde{\underset{\sim}{J}}$ of the Jacobian at $(x, \mu) = (0, 0)$ takes the form

$$\tilde{\underset{\sim}{J}} = -2q_1 + 1 \tag{6.7}$$

which becomes singular at $q_1 = \frac{1}{2}$. The point $(x, \mu) = (0, 0)$ is thus a discontinuous bifurcation point (Figure 6.3a). Furthermore,

$$f_{,\mu} = \frac{1}{2}\operatorname{sgn}(\mu) + \frac{1}{2}\operatorname{sgn}(x - \frac{1}{2}\mu) \tag{6.8}$$

which is discontinuous at the bifurcation point. We therefore construct a linear approximation

$$\tilde{f}_{,\mu} = \frac{1}{2}(2q_2 - 1) + \frac{1}{2}(2q_1 - 1) = q_2 + q_1 - 1 \tag{6.9}$$

The matrix $\left[\tilde{\underset{\sim}{J}} | \tilde{f}_{,\mu}\right]$ has rank $n-1$ at $q_1 = \frac{1}{2}, q_2 = \frac{1}{2}$. A second branch thus crosses the bifurcation point as in the smooth case.

Theorem 3 (Transcritical Bifurcation Theorem)
A transcritical bifurcation of a fixed point of $\dot{\underset{\sim}{x}} = \underset{\sim}{f}(\underset{\sim}{x}; \mu)$ *occurs in the* $\underset{\sim}{x}$–μ *state-control space at* $(\underset{\sim}{x}^*, \mu^*)$ *if the following conditions are satisfied:*

1. $\underset{\sim}{f}(\underset{\sim}{x}^*, \mu^*) = 0$,
2. $det(\tilde{\underset{\sim}{J}}(q_j)) = 0$ *for some set* q_j, *where* $0 \leq q_j \leq 1$,
3. $\left[\tilde{\underset{\sim}{J}} | \tilde{\underset{\sim}{f}}_{,\mu}\right]$ *has rank* $n - 1$,
4. *Two branches exchange stability*

If we smooth the non-smooth system with an arctangent

$$\dot{x} \approx \frac{1}{\pi}\arctan(\frac{1}{2}\varepsilon\mu)\mu - \frac{2}{\pi}\arctan(\varepsilon(x - \frac{1}{2}\mu))(x - \frac{1}{2}\mu) \approx \frac{2}{\pi}\varepsilon(\mu x - x^2),$$

the resulting bifurcation will be a continuous transcritical bifurcation for all ε as can be seen from the expansion around the bifurcation point ($x = 0$, $\mu = 0$). The smoothed system can be transformed to the standard normal form with the time transformation $\tau = \varepsilon t$. The bifurcation in Figure 6.3 is therefore a discontinuous transcritical bifurcation.

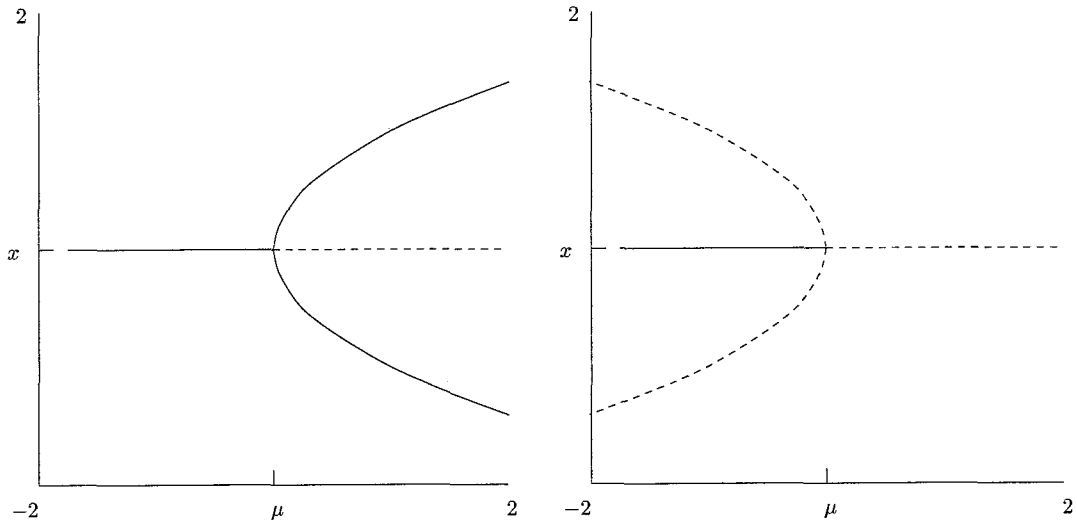

(a) supercritical (b) subcritical

Figure 6.4: pitchfork bifurcation, smooth

6.4 Pitchfork bifurcation

We consider the smooth system

$$\dot{x} = f(x;\mu) = \mu x + \alpha x^3 \tag{6.10}$$

There are three fixed points

$$\begin{array}{ll} x = 0 & \text{trivial point} \\ x = \pm\sqrt{-\frac{\mu}{\alpha}} & \end{array}$$

The Jacobian

$$\underline{J} = \mu + 3\alpha x^2$$

has the single eigenvalues

$$\begin{array}{ll} \lambda = \mu, & \text{at } x = 0 \\ \lambda = -2\mu, & \text{at } x = \pm\sqrt{-\frac{\mu}{\alpha}} \end{array}$$

For $\alpha < 0$ there is a supercritical pitchfork bifurcation (Figure 6.4a) and for $\alpha > 0$ a subcritical pitchfork bifurcation (Figure 6.4b). At a continuous pitchfork bifurcation point, $f_{,\mu}$ does belong to the range of the matrix $\underline{J}$. Hence the matrix $[\underline{J}|f_{,\mu}]$ has rank $n-1$ which is consistent with the fact that two branches intersect at the bifurcation point.

The associated non-smooth system is defined by:

$$\dot{x} = f(x;\mu) = -x + |x + \frac{1}{2}\mu| - |x - \frac{1}{2}\mu| \tag{6.11}$$

There are again three fixed points

$$\begin{array}{ll} x = 0 & \text{trivial point} \\ x = \pm\mu & \text{for } \mu > 0 \end{array}$$

The Jacobian

$$\underline{J} = -1 + \text{sgn}(x + \frac{1}{2}\mu) - \text{sgn}(x - \frac{1}{2}\mu)$$

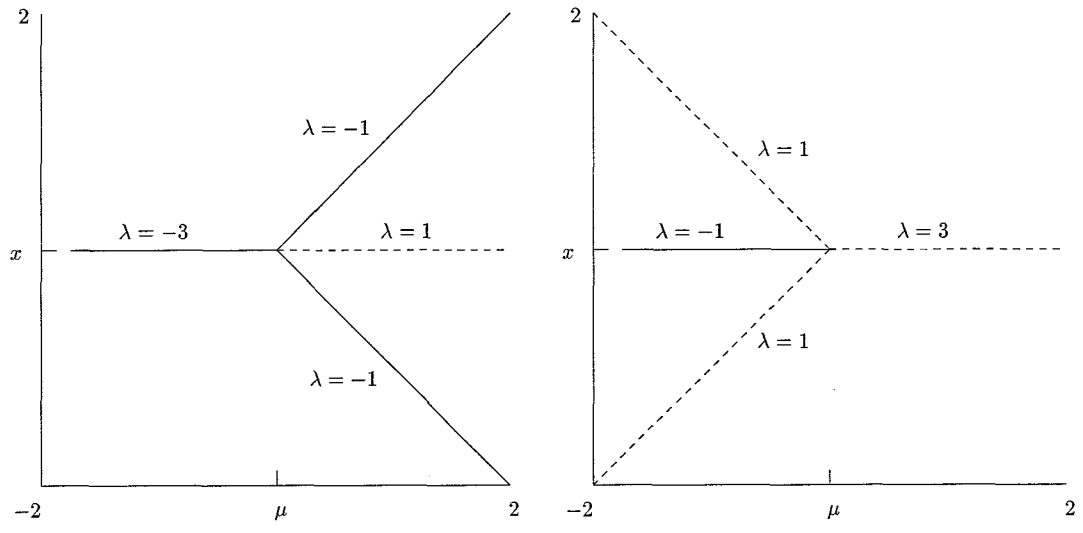

(a) supercritical

(b) subcritical

Figure 6.5: pitchfork bifurcation, discontinuous

has the single eigenvalues

$$\begin{aligned} \lambda &= -3, \quad \text{at } x = 0, \mu < 0 \\ \lambda &= 1, \quad \text{at } x = 0, \mu > 0 \\ \lambda &= -1, \quad \text{at } x = \pm\mu, \mu > 0 \end{aligned}$$

and is discontinuous at $(x, \mu) = (0, 0)$. As there are two hyperplanes where the vector field is discontinuous, we need two parameters for a linear approximation of the Jacobian at $(x, \mu) = (0, 0)$.

$$\underline{\tilde{J}} = -1 + (-2q_1 + 1) - (-2q_2 + 1) = 2(q_2 - q_1) - 1 \tag{6.12}$$

which becomes singular at

$$q_2 - q_1 = \frac{1}{2} \tag{6.13}$$

The point $(x, \mu) = (0, 0)$ is therefore a static bifurcation point. Furthermore,

$$f_{,\mu} = \frac{1}{2}\operatorname{sgn}(x + \frac{1}{2}\mu) + \frac{1}{2}\operatorname{sgn}(x - \frac{1}{2}\mu) \tag{6.14}$$

which is discontinuous at the bifurcation point. We therefore construct a linear approximation

$$\tilde{f}_{,\mu} = \frac{1}{2}(2q_1 - 1) + \frac{1}{2}(2q_2 - 1) = q_1 + q_2 - 1 \tag{6.15}$$

The matrix $\left[\underline{\tilde{J}} | \tilde{f}_{,\mu}\right]$ has rank $n-1$ at $q_1 = \frac{3}{4}, q_2 = \frac{1}{4}$. A second branch thus crosses the bifurcation point as in the smooth case.

The bifurcation diagram is shown in Figure 6.5a for the supercritical pitchfork bifurcation of system 6.11. Similarly, the system

$$\dot{x} = f(x; \mu) = x + |x + \frac{1}{2}\mu| - |x - \frac{1}{2}\mu| \tag{6.16}$$

has a subcritical pitchfork bifurcation (Figure 6.5b). We smooth the non-smooth system 6.11 with an arctangent and apply a Taylor series expansion around ($x = 0$, $\mu = 0$)

$$\begin{aligned} \dot{x} &= -x + |x + \tfrac{1}{2}\mu| - |x - \tfrac{1}{2}\mu| \\ &\approx -x + \tfrac{2}{\pi}\arctan(\varepsilon(x + \tfrac{1}{2}\mu))(x + \tfrac{1}{2}\mu) - \tfrac{2}{\pi}\arctan(\varepsilon(x - \tfrac{1}{2}\mu))(x - \tfrac{1}{2}\mu) \\ &\approx (-1 + \tfrac{4}{\pi}\varepsilon\mu)x - \tfrac{8}{3\pi}\varepsilon^3\mu x^3 \end{aligned}$$

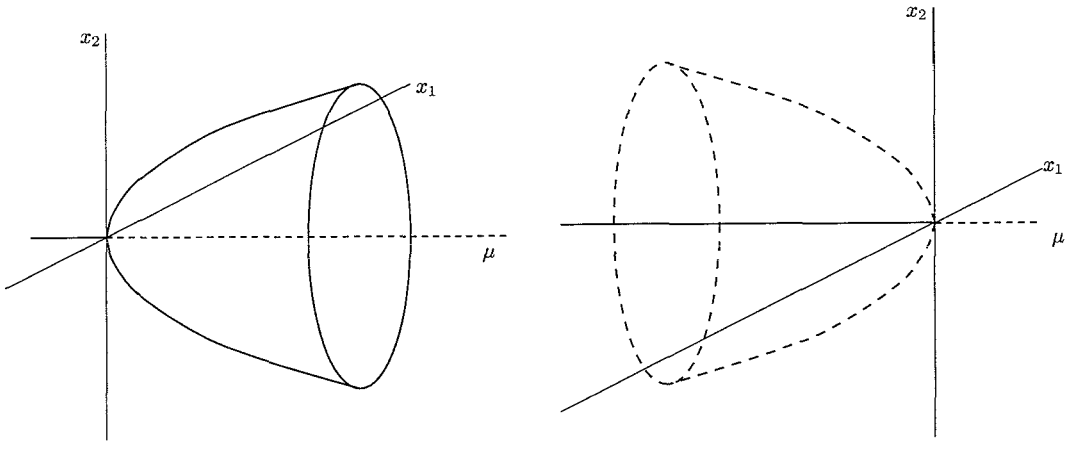

(a) supercritical (b) subcritical

Figure 6.6: Hopf bifurcation, smooth

The resulting bifurcation will be a continuous pitchfork bifurcation with the bifurcation point at $(x = 0, \mu = \frac{\pi}{4\varepsilon})$. The bifurcation point of the smoothed system thus approaches the origin as ε is increased. The bifurcation in Figure 6.5 is therefore a discontinuous pitchfork bifurcation.

Theorem 4 (Pitchfork Bifurcation Theorem)
A pitchfork bifurcation of a fixed point of $\dot{\underset{\sim}{x}} = \underset{\sim}{f}(\underset{\sim}{x}; \mu)$ *occurs in the* $\underset{\sim}{x}$*-*μ *state-control space at* $(\underset{\sim}{x}^*, \mu^*)$ *if the following conditions are satisfied:*

1. $\underset{\sim}{f}(\underset{\sim}{x}^*, \mu^*) = 0$,
2. $det(\underline{\tilde{J}}(q_j)) = 0$ *for some set* q_j, *where* $0 \leq q_j \leq 1$,
3. $\left[\underline{\tilde{J}} | \underset{\sim,\mu}{\tilde{f}}\right]$ *has rank* $n - 1$,
4. *Only one branch exchanges stability.*

6.5 Hopf bifurcation

At a Hopf bifurcation point the fixed point looses its stability and a periodic solution is born. First, we consider the smooth planar system

$$\begin{aligned} \dot{x}_1 &= \mu x_1 - \omega x_2 + (\alpha x_1 - \beta x_2)(x_1^2 + x_2^2) \\ \dot{x}_2 &= \omega x_1 + \mu x_2 + (\beta x_1 + \alpha x_2)(x_1^2 + x_2^2) \end{aligned} \tag{6.17}$$

This system has a fixed point $\underset{\sim}{x} = [x_1, x_2]^T = [0, 0]^T$ and the Jacobian matrix of the linearized system around the fixed point is

$$\underline{J} = \begin{bmatrix} \mu & -\omega \\ \omega & \mu \end{bmatrix}$$

with the eigenvalues

$$\begin{aligned} \lambda_1 &= \mu - i\omega \\ \lambda_2 &= \mu + i\omega \end{aligned}$$

For $\mu < 0$ the fixed point is stable. When μ is increased to $\mu = 0$ the fixed point becomes non-hyperbolic, and for $\mu > 0$, the fixed point becomes unstable. By using the transformation

$$x_1 = r\cos\theta \quad \text{and} \quad x_2 = r\sin\theta \tag{6.18}$$

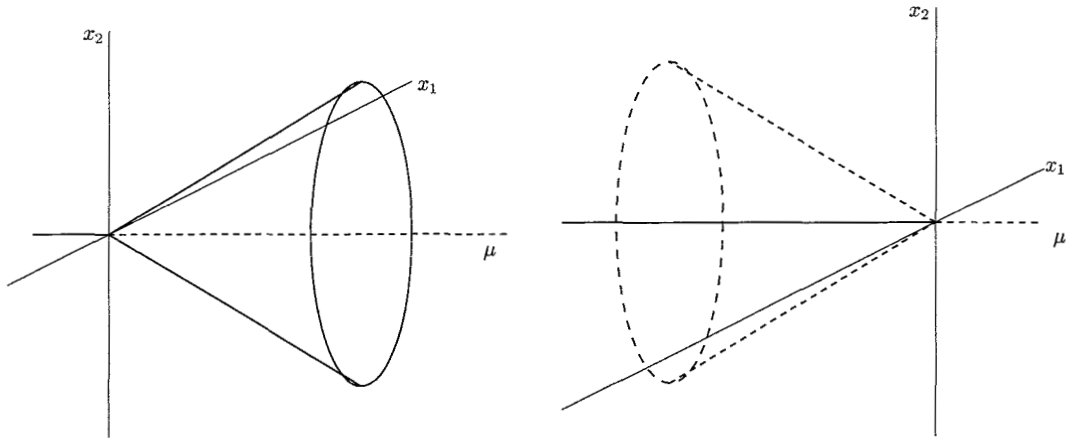

(a) supercritical (b) subcritical

Figure 6.7: Hopf bifurcation, discontinuous

we transform Equation 6.17 into

$$\dot{r} = \mu r + \alpha r^3 \tag{6.19}$$

$$\dot{\theta} = \omega + \beta r^2 \tag{6.20}$$

The trivial fixed point of Equation 6.19 corresponds to the fixed point of Equation 6.17, and the nontrivial fixed point ($r \neq 0$) of Equation 6.19 corresponds to a periodic solution of Equation 6.17. In the latter case, r is the amplitude and $\dot{\theta}$ is the frequency of the periodic solution that is created by the Hopf bifurcation. The transformation by Equation 6.18 thus transforms the Hopf bifurcation into the pitchfork bifurcation. The scenario for the Hopf bifurcation is depicted in Figure 6.6 and the scenario for Equation 6.19 is identical to Figure 6.4 where x should be replaced by r.

We now construct the corresponding non-smooth system

$$\begin{aligned} \dot{x}_1 &= -x_1 - \omega x_2 + \frac{x_1}{\sqrt{x_1^2+x_2^2}}(|\sqrt{x_1^2+x_2^2} + \tfrac{1}{2}\mu| - |\sqrt{x_1^2+x_2^2} - \tfrac{1}{2}\mu|) \\ \dot{x}_2 &= \omega x_1 - x_2 + \frac{x_2}{\sqrt{x_1^2+x_2^2}}(|\sqrt{x_1^2+x_2^2} + \tfrac{1}{2}\mu| - |\sqrt{x_1^2+x_2^2} - \tfrac{1}{2}\mu|) \end{aligned} \tag{6.21}$$

The non-smooth system has the same fixed point as the smooth system with the same stability. We transform Equation 6.21 with the transformation of Equation 6.18 into

$$\dot{r} = -r + |r + \frac{1}{2}\mu| - |r - \frac{1}{2}\mu| \tag{6.22}$$

$$\dot{\theta} = \omega \tag{6.23}$$

The one-dimensional system in Equation 6.22 is identical to the non-smooth pitchfork system in Equation 6.11. The scenario for the discontinuous Hopf bifurcation is depicted in Figure 6.7 and the scenario for Equation 6.22 is identical to Figure 6.5.

Theorem 5 (Hopf Bifurcation Theorem)
A Hopf bifurcation of a fixed point of $\dot{\underset{\sim}{x}} = \underset{\sim}{f}(\underset{\sim}{x};\mu)$ occurs in the $\underset{\sim}{x}$–μ state-control space at $(\underset{\sim}{x}^*, \mu^*)$ if the following conditions are satisfied:

1. $\underset{\sim}{f}(\underset{\sim}{x}^*, \mu^*) = 0$,

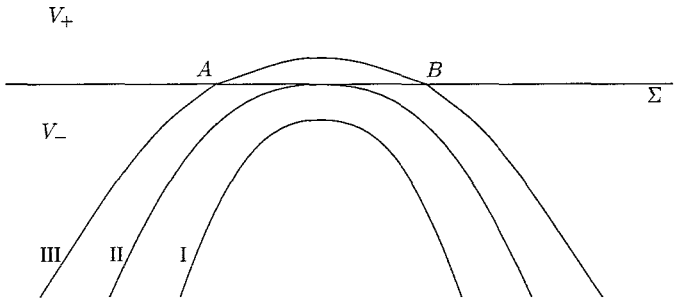

Figure 7.1: Double intersection of a smooth hyperplane

2. $\underline{\tilde{J}}(q_j)$ *has a purely imaginary pair of eigenvalues* $\lambda = \pm\omega i$ *for some set* q_j, *where* $0 \leq q_j \leq 1$

All classical bifurcations of fixed points were discussed in this section and it was shown that there exists a complete parallel between the continuous and discontinuous bifurcations. We will now proceed with bifurcations of periodic solutions.

7 Bifurcations of Periodic Solutions

7.1 Introduction

In the preceding section, the stability of fixed points was discussed. A fixed point looses its stability if the largest eigenvalue of the linearly approximated Jacobian $\underline{\tilde{J}}(q_j)$ passes the imaginary axis for some set q_j. If $\underline{\tilde{J}}$ is constant (independent of q_j), then the bifurcation is a continuous bifurcation. A discontinuous bifurcation of a fixed point is introduced in this paper as a bifurcation for which $\underline{\tilde{J}}$ varies for varying q_j.

A periodic solution can be envisaged as a fixed point of a Poincaré map P on a Poincaré section. The results on bifurcations of fixed points are thus useful for the investigation of bifurcations of periodic solutions. The stability of a periodic solution is determined by its Floquet multipliers λ_i $(i = 1,...,n)$, which are the eigenvalues of the fundamental solution matrix $\underline{\Phi}(T + t_0, t_0)$. The Floquet multipliers are the generalization of the eigenvalues at a fixed point. Because, in an autonomous system the phase of the solution is undefined, one of the Floquet multipliers equals unity. The periodic solution is stable if all Floquet multipliers (not associated with the phase in the autonomous case) lie within the unit circle. If one or more Floquet multipliers lie outside the unit circle, then the periodic solution is unstable. The periodic solution varies (as well as its Floquet multipliers) as a control parameter of the system is varied. The periodic solution exchanges stability when the largest Floquet multiplier crosses the unit circle. This is called a bifurcation of a periodic solution.

In Section 3 we elaborated how fundamental solution matrices of discontinuous systems can jump as the flow crosses a hyperplane. Jumps of the Jacobian of fixed points can lead to discontinuous bifurcations as was outlined in the preceding section. The question arises: can jumps in the fundamental solution matrix cause discontinuous bifurcations of periodic solutions?

We consider the following scenario (Figure 7.1). The hyperplane Σ defines a discontinuity and divides the state space in the two subspaces V^+ and V^-. The vector field is discontinuous on Σ $(\underset{\sim}{f}_- \neq \underset{\sim}{f}_+)$ but the form of Σ is smooth. A periodic solution I does not cross Σ when a control parameter μ is smaller than a critical value $\mu < \mu^*$. The solution II touches Σ at $\mu = \mu^*$. For $\mu > \mu^*$, the solution III crosses Σ twice at points A and B. Let us assume that solution I comes infinitely close to Σ but does not touch it and that solution III stays an infinitely small time in V^+ but crosses Σ twice. The solutions I and III are therefore (almost) identical, but the fundamental solution matrix of solution III will jump twice with saltation matrices $\underline{S}_A$ and $\underline{S}_B$. The crossings occur at $t_A = t_B = t_\Sigma$ as the flow stays an infinitely small time in V^+. We can now express the

fundamental solution matrix of $\underline{\Phi}_{III}$ into $\underline{\Phi}_I$ with a conversion matrix, a concept newly introduced in Subsection 3.4,

$$\underline{\Phi}_{III}(T+t_0,t_0) = \underline{\Phi}_I(T+t_0,t_0)\underline{C}(T+t_0,t_0) \tag{7.1}$$

with the conversion matrix

$$\underline{C}(T+t_0,t_0) = \underline{\Phi}_I^{-1}(t_\Sigma+t_0,t_0)\underline{S}_B\underline{S}_A\underline{\Phi}_I(t_\Sigma+t_0,t_0) \tag{7.2}$$

However, from Equations 3.25 and 3.26 we conclude that $\underline{S}_B = \underline{S}_A^{-1}$, thus $\underline{C}(T+t_0,t_0) = \underline{I}$. The fundamental solution matrix of solution III is therefore identical to solution I. This scenario, in which a single hyperplane is crossed twice, can consequently not lead to a bifurcation of a periodic solution if $\underline{S}_A$ is non-singular. The singular case arises in sliding mode problems (for instance in Section 7.8).

The preceding scenario did not lead to a bifurcation because the saltation matrix over a hyperplane is equal to the inverse of the saltation matrix in opposite direction over the same hyperplane at that point. We will study a second scenario which is depicted in Figure 7.2. The hyperplane Σ is now non-smooth and consists of two parts Σ_A and Σ_B. The flow III enters V_+ by crossing Σ_A at point A and leaves V_+ by crossing Σ_B at point B. The saltation matrix $\underline{S}_A$ is (in general) not equal to $\underline{S}_B$. Consequently, the conversion matrix will not be equal to the identity matrix. Thus, at $\mu = \mu^*$, the fundamental solution matrix over the period time $\underline{\Phi}_{II}(T+t_0,t_0)$ will jump from $\underline{\Phi}_I(T+t_0,t_0)$ to $\underline{\Phi}_{III}(T+t_0,t_0)$. The theory of linear approximation (developed for fixed points) is now applicable, as a periodic solution is a fixed point of a Poincaré map. We combine the two saltations $\underline{S}_{BA} = \underline{S}_B\underline{S}_A$. From Section 5 we know that the theory of linear approximation also applies to the saltation matrix. Therefore

$$\tilde{\underline{S}}_{BA} = \underline{I} + q(\underline{S}_{BA} - \underline{I}) \tag{7.3}$$

which implies that the conversion matrix can also be approximated linearly

$$\begin{aligned}\tilde{\underline{C}}(T+t_0,t_0) &= \underline{\Phi}_I^{-1}(t_\Sigma+t_0,t_0)\tilde{\underline{S}}_{BA}\underline{\Phi}_I(t_\Sigma+t_0,t_0)\\ &= \underline{I} + q(\underline{C}(T+t_0,t_0) - \underline{I})\end{aligned} \tag{7.4}$$

We introduce the *fundamental solution matrix of linear approximation* $\tilde{\underline{\Phi}}$ at $\mu = \mu^*$ which varies between $\underline{\Phi}_I$ and $\underline{\Phi}_{III}$ with the parameter q.

$$\tilde{\underline{\Phi}} = q(\underline{\Phi}_{III}(T+t_0,t_0) - \underline{\Phi}_I(T+t_0,t_0)) + \underline{\Phi}_I(T+t_0,t_0) \tag{7.5}$$

A bifurcation occurs at $\mu = \mu^*$ if one of the eigenvalues of $\tilde{\underline{\Phi}}$ lie on the unit circle for some q.

The Floquet multipliers thus jump at $\mu = \mu^*$, with a path given by the eigenvalues of $\tilde{\underline{\Phi}}$. A Floquet multiplier can jump from inside the unit circle to outside the unit circle causing a discontinuous bifurcation. Where the Floquet multiplier crossed the unit circle during its jump is determined by $\tilde{\underline{\Phi}}$. The jumping Floquet multiplier can also jump form outside the unit circle to another point outside the unit circle in the complex plane. Whether we have to do with a bifurcation depends on the path of the Floquet multiplier during its jump. It could have jumped from one point to the other without passing the unit circle or it could have passed it twice (causing two discontinuous bifurcations). The fundamental solution of linear approximation is thus essential for the determination of the existence and type of bifurcation.

Theorem 6 (Bifurcation Theorem of Periodic Solutions)
Let the flow $\underset{\sim}{x}(t,t_0)$ with initial condition $\underset{\sim}{x}(t_0,t_0) = \underset{\sim}{x}_0$ be a periodic solution, $\underset{\sim}{x}(T+t_0,t_0) = \underset{\sim}{x}(t,t_0)$, with period time T. The periodic solution and period time depend on a scalar control parameter μ. Let $H(\underset{\sim}{x},T,\mu) = 0$ define a branch of periodic solutions under the variation of μ and let s be the arc-length of the branch. Let $\underline{\Phi}_T^+$ be the fundamental solution matrix of the periodic solution at $\lim_{s\downarrow s^*}\underline{\Phi}_T$ and $\underline{\Phi}_T^-$ at $\lim_{s\uparrow s^*}\underline{\Phi}_T$. Let the Floquet multipliers of $\underline{\Phi}_T^+$ be $\lambda_i^+ =$

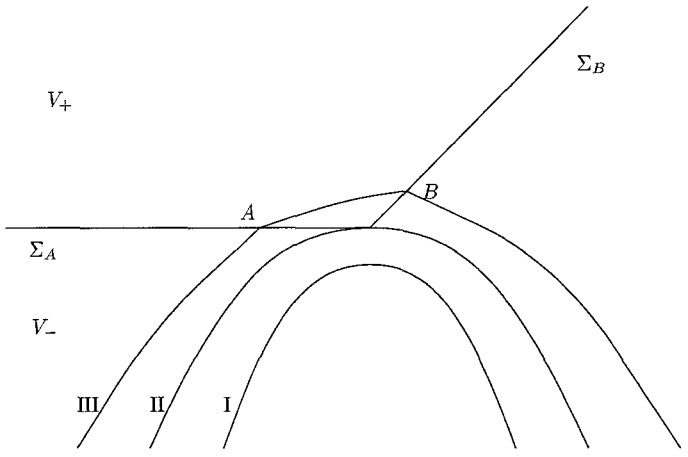

Figure 7.2: Double intersection of a non-smooth hyperplane

$\{m_1^+, m_2^+, ..., m_{n-1}^+, 1\}$ *and of* $\underline{\Phi}_T^-$ *be* $\lambda_i^- = \{m_1^-, m_2^-, ..., m_{n-1}^-, 1\}$, *where the last Floquet multiplier is associated with the phase of the autonomous system.*
Let $\tilde{\underline{\Phi}}(q)$ *be the fundamental solution matrix of linear approximation*

$$\tilde{\underline{\Phi}}(q) = q(\underline{\Phi}_T^+ - \underline{\Phi}_T^-) + \underline{\Phi}_T^- \tag{7.6}$$

A **discontinuous bifurcation of a periodic solution** *exist on the branch H at* $s = s^*$ *if*

$$det(\tilde{\underline{\Phi}}(q) - \lambda \underline{I}) = 0 \tag{7.7}$$

for some q *and* λ, *where* $0 \leq q \leq 1$ *and* $|\lambda| = 1$

Remarks. The above theorem is implicit as Equation 7.7 is implicit in q and λ. The value of q at which the bifurcation occurs is not interesting but has to be solved numerically to find λ. The bifurcation becomes continuous if $\underline{\Phi}_T^+ = \underline{\Phi}_T^-$.

7.2 Fold bifurcation; Trilinear spring system

In this section we will treat the discontinuous fold bifurcation. The forced oscillation of a damped mass on a spring with cubic term leads to the Duffing equation [9, 8, 18, 19]. The Duffing equation is the classical example where the backbone curve of the harmonic peak is bended and two folds (also called turning point bifurcations) are born. In our example, we will consider a similar mass-spring-damper system, where the cubic spring is replaced by a trilinear spring. Additionally, trilinear damping is added to the model. The trilinear damping will turn out to be essential for the existence of a *discontinuous* fold bifurcation.

The model is very similar to the model of Natsiavas [16, 17] but the transitions from contact with the support to no contact are different from Natsiavas. The model of Natsiavas switches as the position of the mass passes the contact distance (in both transition directions). In our model, contact is made when the position of the mass passes the contact distance, and contact is lost when the contact force becomes zero.

We consider the system depicted in Figure 7.3. The model is similar to the discontinuous support of Example II in Subsection 4.2 but now has two supports on equal contact distances x_c. The supports are first-order systems which relax to their original state if there is no contact with the mass. If we assume that the relaxation time of the supports is much smaller than the time interval between two impacts, we can neglect the free motion of the supports. It is thus assumed that the supports are at rest at the moment of impact. This is not an essential assumption but simplifies our treatment as the system reduces to a second-order equation.

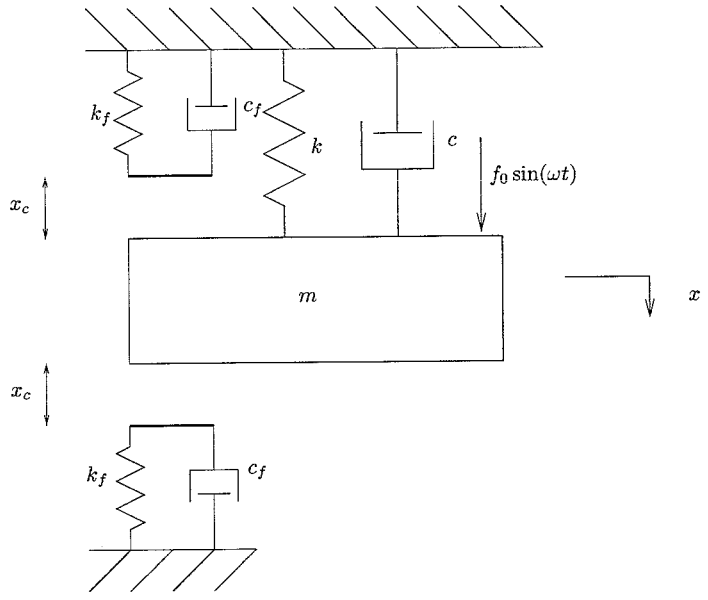

Figure 7.3: Trilinear system

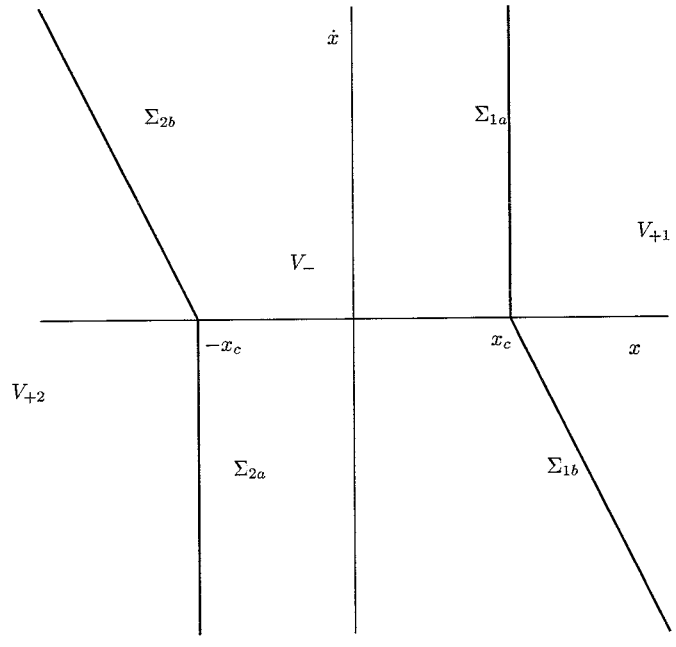

Figure 7.4: Subspaces of the trilinear system

The second-order differential equation of this system is

$$m\ddot{x} + C(\dot{x}) + K(x) = f_0 \sin(\omega t) \tag{7.8}$$

where

$$K(x) = \begin{cases} kx & \in V_- \\ kx + k_f(x - x_c) & \in V_{+1} \\ kx + k_f(x + x_c) & \in V_{+2} \end{cases} \tag{7.9}$$

is the trilinear restoring force and

$$C(\dot{x}) = \begin{cases} c\dot{x} & \in V_- \\ (c + c_f)\dot{x} & \in V_{+1} \cup V_{+2} \end{cases} \tag{7.10}$$

is the trilinear damping force. The state space is divided into three subspaces V_-, V_{+1} and V_{+2} (Figure 7.4).

If the mass is in contact with the lower support, then the state is in space V_{+1}

$$V_{+1} = \{[x, \dot{x}]^T \in I\!R^2 \mid x > x_c, k_f(x - x_c) + c_f\dot{x} \geq 0\},$$

whereas if the mass is in contact with the upper support, then the state is in space V_{+2}

$$V_{+2} = \{[x, \dot{x}]^T \in I\!R^2 \mid x < -x_c, k_f(x + x_c) + c_f\dot{x} \leq 0\}.$$

If the mass is not in contact with one of the supports, then the state is in space V_- defined by

$$V_- = \{[x, \dot{x}]^T \in I\!R^2 \mid x \notin (V_{+1} \cup V_{+2})\}$$

The hyperplane Σ_1 between V_- and V_{+1} consists of two parts Σ_{1a} and Σ_{1b}. The part Σ_{1a} is defined by the indicator equation

$$h_{1a} = x - x_c = 0 \tag{7.11}$$

which defines the transition from V_- to V_{+1} because contact is made when x becomes larger than x_c. The part Σ_{1a} is defined by the indicator equation

$$h_{1b} = k_f(x - x_c) + c_f\dot{x} = 0 \tag{7.12}$$

which defines the transition from V_{+1} back to V_- as contact is lost when the support-force becomes zero (the support can only push, not pull on the mass). Similarly, the hyperplane Σ_2 between V_- and V_{+2} consists of two parts Σ_{2a} and Σ_{2b} defined by the indicator equations

$$h_{2a} = x + x_c = 0 \tag{7.13}$$

$$h_{2b} = k_f(x + x_c) + c_f\dot{x} = 0 \tag{7.14}$$

Like we have done in Subsection 4.2 we can construct the saltation matrices. The saltation matrices are of course similar to those of Subsection 4.2

$$\underline{S}_{1a} = \begin{bmatrix} 1 & 0 \\ -\frac{c_f}{m} & 1 \end{bmatrix} \tag{7.15}$$

$$\underline{S}_{1b} = \underline{I} \tag{7.16}$$

$$\underline{S}_{2a} = \begin{bmatrix} 1 & 0 \\ -\frac{c_f}{m} & 1 \end{bmatrix} \tag{7.17}$$

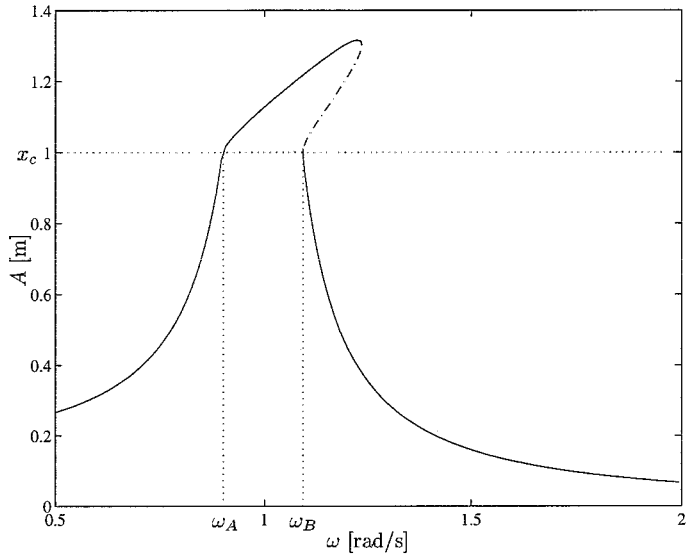

Figure 7.5: Response diagram of trilinear spring system

$$\underline{S}_{2b} = \underline{I} \tag{7.18}$$

The hyperplanes Σ_1 and Σ_2 are non-smooth. The saltation matrices are not each others inverse, $\underline{S}_{1a} \neq \underline{S}_{1b}^{-1}$ and $\underline{S}_{2a} \neq \underline{S}_{2b}^{-1}$. According to Subsection 7.1 we now have all the ingredients for the existence of a discontinuous bifurcation.

The response diagram of the trilinear system is shown in Figure 7.5 for varying forcing frequencies with the amplitude A of x on the vertical axis. Stable branches are indicated by solid lines and unstable branches by dashed-dotted lines. The parameter values are given in Appendix B.

There is no contact with the support for amplitudes smaller than x_c and the response curve is just the linear harmonic peak. For amplitudes above x_c there will be contact with the support which will cause a hardening behaviour of the response curve. The backbone curve of the peak bends to the right like the Duffing system with a hardening spring. The amplitude becomes equal to x_c twice at $\omega = \omega_A$ and $\omega = \omega_B$, on both sides of the peak, and corners of the response curve can be seen at these points. The orbit touches the corners of Σ_1 and Σ_2 for $A = x_c$, like solution II in Figure 7.2. The Floquet multipliers can thus jump at those points. The magnitude of the Floquet multipliers is shown in Figure 7.6. The two Floquet multipliers are complex conjugate (with the same magnitude) for $A < x_c$. The pair of Floquet multipliers jump at ω_A but do not jump through the unit circle. However, at $\omega = \omega_B$ the complex pair jumps to two distinct real multipliers, one with a magnitude bigger than one. A Floquet multiplier thus jumped through the unit circle causing a *discontinuous fold bifurcation.*

Damping of the support is essential for the existence of this discontinuous fold bifurcation. For $c_f = 0$, all saltation matrices would be equal to the identity matrix and the corner between Σ_{1a} and Σ_{1b} would disappear (and also between Σ_{2a} and Σ_{2b}); thus no discontinuous bifurcation could take place and the fold bifurcation would be continuous. The model of Natsiavas [16, 17] did not contain a *discontinuous* fold bifurcation because the transitions were modeled such that $\underline{S}_{1a} = \underline{S}_{1b}^{-1}$ and $\underline{S}_{2a} = \underline{S}_{2b}^{-1}$.

7.3 Infinitely unstable periodic solutions

In the preceding subsection we studied the discontinuous fold bifurcation, where a Floquet multiplier jumped over the unit circle to a finite value. In this subsection we will study a discontinuous fold bifurcation where the Floquet multiplier jumps to infinity. This results in an infinitely unsta-

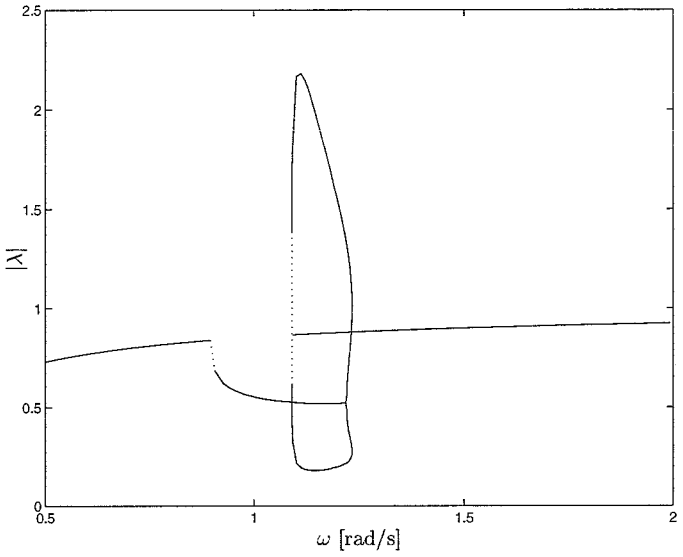

Figure 7.6: Floquet multipliers

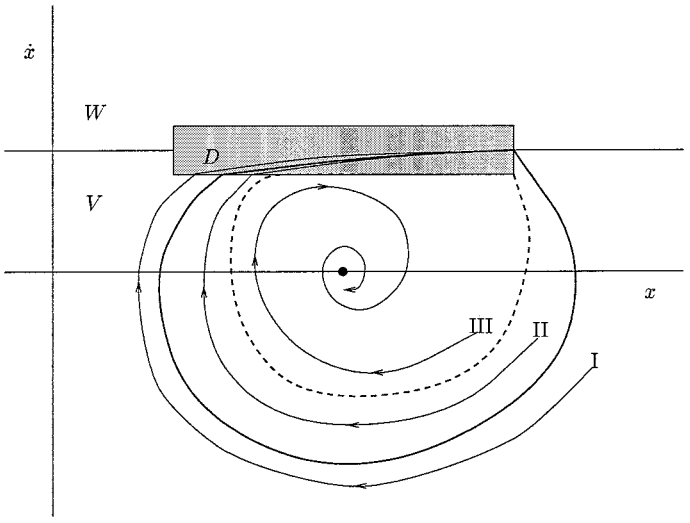

Figure 7.7: Phase plane

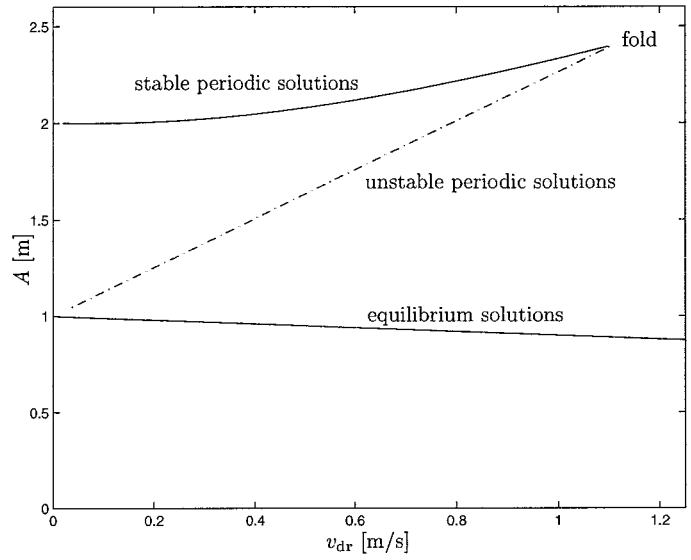

Figure 7.8: Bifurcation diagram of the block-on-belt model

ble periodic solution.

We consider again the block-on-belt model of Subsection 4.1 depicted in Figure 4.1, but now for positive damping $c > 0$. The equilibrium solution of system 4.1 is given by

$$\underset{\sim}{x}_{eq} = \begin{bmatrix} \frac{F_{\text{slip}} - cv_{\text{dr}}}{k} \\ v_{\text{dr}} \end{bmatrix} \tag{7.19}$$

and is stable for positive damping ($c > 0$).

The model also exhibits stable periodic stick-slip oscillations. In Subsection 4.1 it was shown that the saltation matrix for the transition from slip to stick is given by (Equation 4.9)

$$\underline{S}_{\alpha} = \begin{bmatrix} 1 & 0 \\ 0 & 0 \end{bmatrix},$$

which is singular. The conversion matrix and fundamental solution matrix will thus also be singular. The periodic solution has two Floquet multipliers, of which one is always equal to unity as the system is autonomous. The singularity of the fundamental solution matrix implies that the remaining Floquet multiplier has to be equal to zero, independent of any system parameter. The Floquet multipliers of the stable periodic solution of this system are thus $\lambda_{\text{stable}} = (1, 0)$.

The stable limit cycle is sketched in the phase plane in Figure 7.7 (bold line). The equilibrium position is also stable and indicated by a dot. The space D is enlarged in Figure 7.7 to make it visible but is infinitely small in theory and is taken very small in numerical calculations.

A flow outside the stable limit cycle, like flow I in Figure 7.7, will spiral inwards to the stable limit cycle and reach the stick-phase D. The stick-phase will bring the flow exactly on the stable limit cycle as it is infinitely small. Every point in D is thus part of the basin of attraction of the stable limit cycle.

Flow II starts inside the stable limit cycle and spirals around the equilibrium position and hits D where-after it is on the stable limit cycle. But a flow inside the stable limit cycle might also spiral around the equilibrium position and not reach the stick phase D (flow III). It will then be attracted to the equilibrium position.

A flow inside the stable limit cycle can thus spiral outwards to the stable limit cycle, like flow II, or inwards to the equilibrium position (flow III). Consequently, there must exist a boundary of attraction between the two attracting limit sets. This boundary is the unstable limit cycle

sketched by a dashed line in Figure 7.7. Whether a flow is attracted to the stable limit cycle or to the equilibrium point depends on the attainment of the flow to D. The unstable limit cycle is thus defined by the flow in V which hits the border of D tangentially. Another part of the unstable limit cycle is along the border of D as flows in D will attract to the stable limit cycle and just outside D to the equilibrium position. This part of the unstable limit cycle is thus a sliding mode along a discontinuity as discussed in Section 2. The flow on either side of the sliding mode is repulsing from it. It is thus a repulsion sliding mode. The flow starting from a point on a repulsion sliding mode is not unique as was discussed in Section 2. This causes the unstable solution to be infinitely unstable. As the flow is infinitely unstable, it is not possible to calculate it in forward time. However, calculation of the flow in backward time is possible. The vector field in backward time is identical to forward time but opposite in direction. The repulsion sliding mode in forward time will turn into an attraction sliding mode in backward time. The flow starting from a point on the unstable limit cycle will move counter-clockwise in the phase-plane in backward time and hit the border of D. It will slide along the border of D until the vector field in V becomes parallel to D, and will then bend off in V. Any flow starting from a point close to that starting point will hit D and leave D at exactly the same point. Information about where the flow came from is thus lost through the attracting sliding mode. In other words: the saltation matrix of the transition from V to D during backward time is singular. The fundamental solution matrix will thus be singular in backward time because it contains an attracting sliding mode. The Floquet multipliers of the unstable limit cycle in backward time are therefore 1 and 0. The Floquet multipliers in forward time must be their reciprocal values. The second Floquet multiplier is thus infinity, $\lambda_{\text{unstable}} = (1, \infty)$, which of course must hold for an infinitely unstable periodic solution.

The bifurcation diagram of the system is shown in Figure 7.8 with the velocity of the belt v_{dr} as control parameter and the amplitude A on the vertical axis. The equilibrium branch and the stable and unstable periodic branches are depicted. The unstable branch is of course located between the stable periodic branch and the equilibrium branch as can be inferred from Figure 7.7. The stable and unstable periodic branches are connected through a fold bifurcation point. The second Floquet multiplier jumps from $\lambda = 0$ to $\lambda = \infty$ at the bifurcation point, and thus through the unit circle. The fold bifurcation is therefore a discontinuous fold bifurcation. The fold bifurcation occurs when v_{dr} is such that a flow which leaves the stick phase D, transverses V, and hits D tangentially (like the unstable periodic solution). The stable and unstable periodic solutions coincide at this point. Note that there exists again a corner of hyperplanes at this point as in Figure 7.2. The saltation matrices are not each others inverse, $\underline{S}_\alpha \underline{S}_\beta \neq \underline{I}$, which is essential for the existence of a discontinuous bifurcation.

A similar model was studied in [28] with a very accurately smoothed friction curve. The stable branch was followed for increasing v_{dr} but the fold bifurcation could not be rounded to proceed on the unstable branch. As the unstable branch is infinitely unstable in theory, it is extremely unstable for the smoothed system. The branch can thus not be followed in forward time if the friction model is approximated accurately.

The stable branch in Figure 7.8 was followed in forward time up to the bifurcation point. The path-following algorithm was halted and restarted in backward time to follow the unstable branch.

This section showed that infinitely unstable periodic solutions come into being through repulsion sliding modes. Filippov theory turns out to be essential for the understanding of infinitely unstable periodic solutions. Infinitely unstable periodic solutions and their branches can be found through backward integration. Smoothing of a discontinuous model is not sufficient to obtain a complete bifurcation diagram of a discontinuous system as infinitely unstable branches cannot be found.

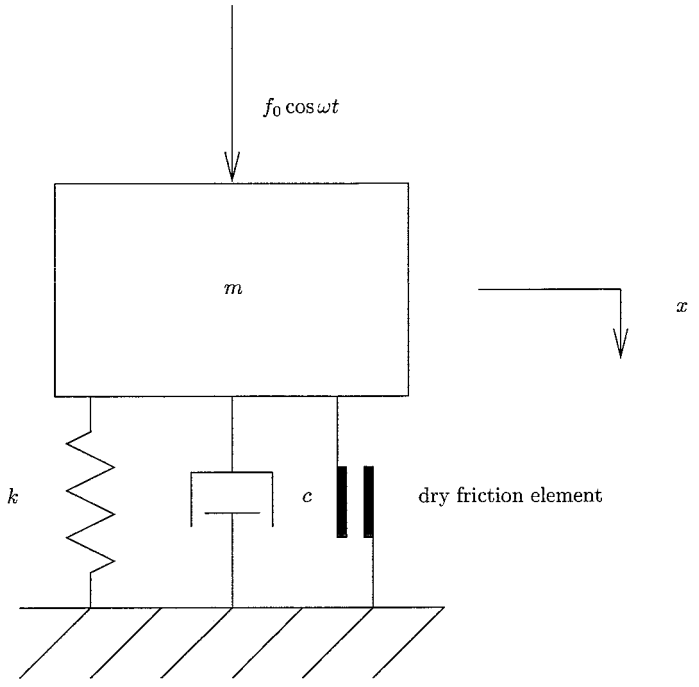

Figure 8.1: Forced vibration with dry friction

8 Symmetry-Breaking Bifurcation; Forced Vibration with Dry Friction

The second type of bifurcation of a periodic solution which will be studied in this paper is the *symmetry-breaking bifurcation.* Suppose a non-autonomous time-periodic system has the following symmetry property (also called *inversion symmetry*)

$$\underset{\sim}{f}(t, \underset{\sim}{x}) = -\underset{\sim}{f}(t + \frac{1}{2}T, -\underset{\sim}{x}), \tag{8.1}$$

where T is the period. If $\underset{\sim}{x}_1(t) = \underset{\sim}{x}(t)$ is a periodic solution of the system, then also $\underset{\sim}{x}_2(t) = -\underset{\sim}{x}(t + \frac{1}{2}T)$ must be a periodic solution. The periodic solution is called *symmetric* if $\underset{\sim}{x}_1(t) = \underset{\sim}{x}_2(t)$ and asymmetric if $\underset{\sim}{x}_1(t) \neq \underset{\sim}{x}_2(t)$. When a Floquet multiplier crosses the unit circle through $+1$, the associated bifurcation depends on the nature of the periodic solution prior to the bifurcation. Suppose that the periodic solution prior to the bifurcation is a symmetric solution. Then, if the bifurcation breaks the symmetry of the periodic solution, it is called a symmetry-breaking bifurcation [18].

We will show in this section that symmetry-breaking bifurcations can also be discontinuous. Consider the forced vibration of the system depicted in Figure 8.1. The mass is supported by a spring, damper and dry friction element. The parameter values are given in Appendix C. The equation of motion reads

$$m\ddot{x} + c\dot{x} + kx = f_{fric}(\dot{x}, x) + f_0 \cos \omega t \tag{8.2}$$

with the friction model

$$f_{fric}(\dot{x}, x) = \begin{cases} -F_{\text{slip}} \operatorname{sgn}(\dot{x}), & \dot{x} \neq 0 \quad \text{slip} \\ \min(|kx - f_0 \cos \omega t|, F_{\text{stick}}) \operatorname{sgn}(kx - f_0 \cos \omega t), & \dot{x} = 0 \quad \text{stick} \end{cases} \tag{8.3}$$

It can be verified that this system has the symmetry property of Equation 8.1.

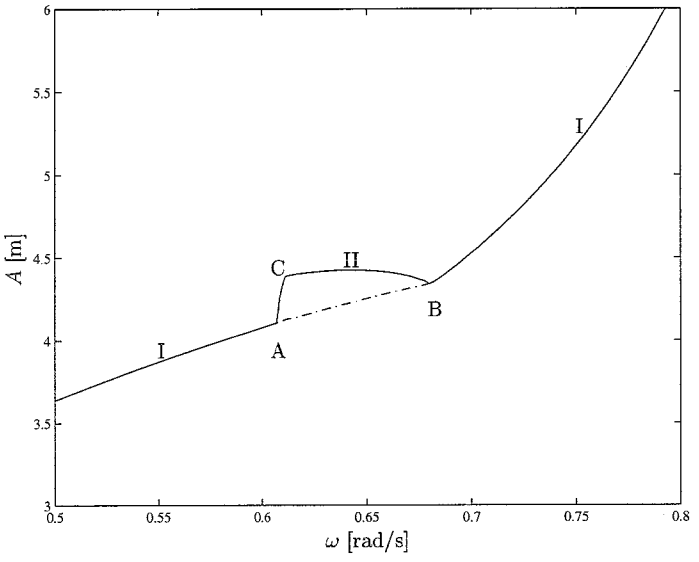

Figure 8.2: Bifurcation diagram of forced vibration with dry friction

The bifurcation diagram of this system is depicted in Figure 8.2 and consists of a branch I which is partly unstable and branch II which bifurcates from branch I. For large amplitudes, the influence of the dry friction element will be much less than the linear elements. Branch I near the resonance frequency, $\omega_{\text{res}} = \sqrt{k/m} = 1$ [rad/s], will therefore be close the harmonic resonance peak of a linear one degree-of-freedom system. The periodic solutions on branch I near ω_{res} are symmetric. The periodic solutions are at only one point of time in the stick phase during one oscillation. The Floquet multipliers on this part of branch I are complex (Figure 8.3). The system thus behaves 'almost linear'.

If this part of branch I with 'almost linear' symmetric solutions is followed to frequencies below ω_{res}, then bifurcation point B is met. At bifurcation point B, the symmetric branch I becomes unstable and a second branch II with asymmetric solutions is created. In fact, on the bifurcated asymmetric branch exist two distinct solutions $\underset{\sim}{x}_1(t) \neq \underset{\sim}{x}_2(t)$ which have the same amplitude. The asymmetric solutions stay a finite time in the stick phase. One Floquet multiplier is consequently equal to zero. The Floquet multipliers at B are set-valued and pass +1. Point B is therefore a *discontinuous symmetry-breaking bifurcation.*

Branch II encounters a jump of the Floquet multipliers at point C but the set-valued Floquet multipliers remain within the unit circle. Point C is therefore not a bifurcation point but the path of branch II is non-smooth at C due to the jump of the Floquet-multipliers.

The asymmetric branch meets the symmetric branch again at point A. The Floquet multipliers pass +1 without a jump and point A is therefore a continuous symmetry bifurcation. Remark that the branch I behaves smooth at bifurcation A and non-smooth at bifurcation B.

9 Flip Bifurcation; Forced Stick-slip System

Another type of bifurcation of a periodic solution is the *flip bifurcation* which is characterized by a Floquet multiplier which is passing the unit circle through -1. A discontinuous flip bifurcation will be studied in this section which occurs in a forced block-on-belt model taken from Yoshitake and Sueoka [29]. The model is identical to the block-on-belt model of Subsection 4.1 (Figure 4.1) without linear damping and a different friction model. Additionally, the mass is forced periodically. The parameter values are given in Appendix D. The equation of motion reads

$$m\ddot{x} + kx = f_{fric}(v_{\text{rel}}, x) + f_0 \cos \omega t \tag{9.1}$$

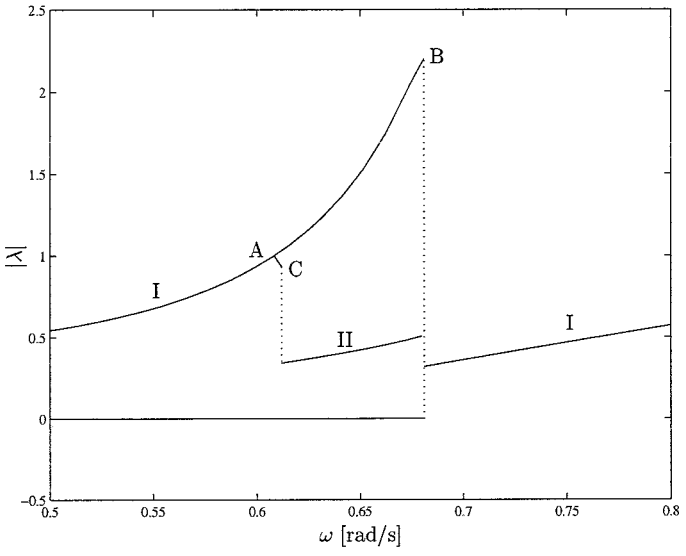

Figure 8.3: Floquet multipliers

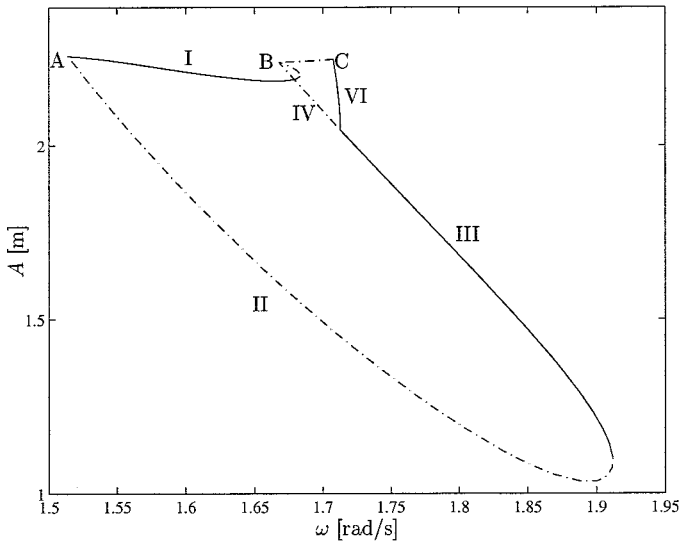

Figure 9.1: Bifurcation diagram of the forced stick-slip system

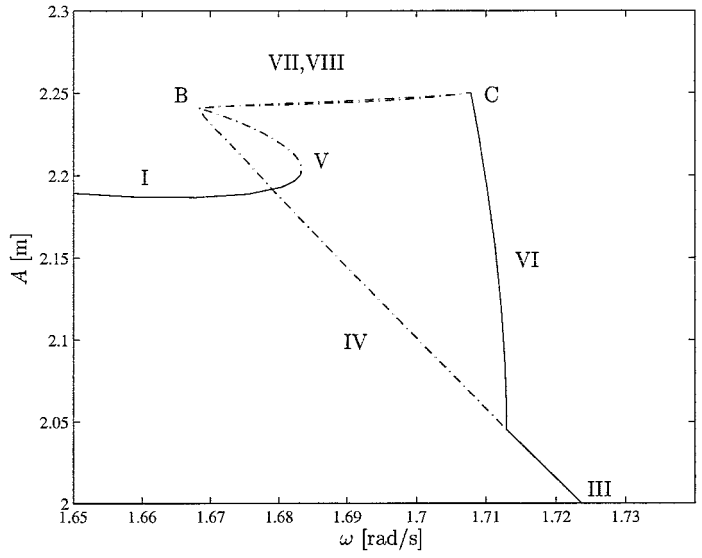

Figure 9.2: Bifurcation diagram of the forced stick-slip system

with $v_{\mathrm{rel}} = \dot{x} - v_{\mathrm{dr}}$. The friction model reads

$$f_{fric}(v_{\mathrm{rel}}, x) = \begin{cases} -\alpha_0 \operatorname{sgn}(v_{\mathrm{rel}}) + \alpha_1 v_{\mathrm{rel}} - \alpha_3 v_{\mathrm{rel}}^3, & v_{\mathrm{rel}} \neq 0 \quad \text{slip} \\ \min(|kx - f_0 \cos\omega t|, \alpha_0) \operatorname{sgn}(kx - f_0 \cos\omega t), & v_{\mathrm{rel}} = 0 \quad \text{stick} \end{cases} \tag{9.2}$$

This model has been analyzed numerically with the switch-model as in Subsection 4.1 and [13].

The resonance curve of this model has been published by Yoshitake and Sueoka [29] for $0.2 \leq \omega \leq 4$. The 1/2-subharmonic closed resonance curve is of special interest and depicted in Figure 9.1 and a part is enlarged in Figure 9.2. The real part of largest Floquet multiplier (in magnitude) is depicted in Figure 9.3. All Floquet multipliers are real except on a part of branch III. Stable branches are denoted by solid lines and unstable branches by dashed-dotted lines. Jumps of the Floquet multiplier (set-valued Floquet multipliers) are denoted by dotted lines.

The 1/2-subharmonic closed resonance curve possesses multiple discontinuous and continuous bifurcations. Branches I-V are period-2 solutions, branches VI and VII are period-4, and branch VIII is period-8. A discontinuous fold bifurcation at point A connects the stable branch I to the unstable branch II and its largest Floquet multiplier jumps through +1. The stable branch I folds smoothly into branch V and stability is exchanged. At point B, the unstable branch V is folded into the unstable branch IV *without exchanging stability.* The set-valued Floquet multiplier crosses the unit circle twice as it jumps from branch V to branch IV. It first passes +1 causing a fold bifurcation and then passes -1 causing a flip bifurcation. A flip bifurcation causes a period-doubled branch to bifurcate from the main branch. Branches I and V are period-2 and branch VII emanates indeed from point B and is period-4. But branch VIII also bifurcates from B and is period-8. This is not in conformity with the bifurcation theory for smooth systems.

A better understanding of the phenomenon can be obtained by looking at the Poincaré map depicted in Figure 9.4. In fact, the 'full' Poincaré map is a mapping from $\mathbb{R}^2$ to $\mathbb{R}^2$ which cannot easily be visualized. Instead, a section of this map is depicted with the displacement $x_n = x(nT)$, where $T = 2\pi/\omega$, on the abscissa and the displacement after two periods x_{n+2} on the ordinate. The velocity $\dot{x}_n$ is iterated with a Newton-Raphson method to be equal to $\dot{x}_{n+2}$. Fixed points of this reduced map are periodic solutions with period-2 (or period-1) as holds $x(nT) = x((n+2)T)$ and $\dot{x}(nT) = \dot{x}((n+2)T)$. The map is calculated for $\omega = 1.67587$ [rad/s] which is just to right of the bifurcation point B. It can be seen that there are three fixed points which corresponds to the periodic solutions at the branches I, IV and V. Moreover exposes the map a *tent structure* with a peak between the fixed points IV and V. Although this is a section of a higher dimensional map,

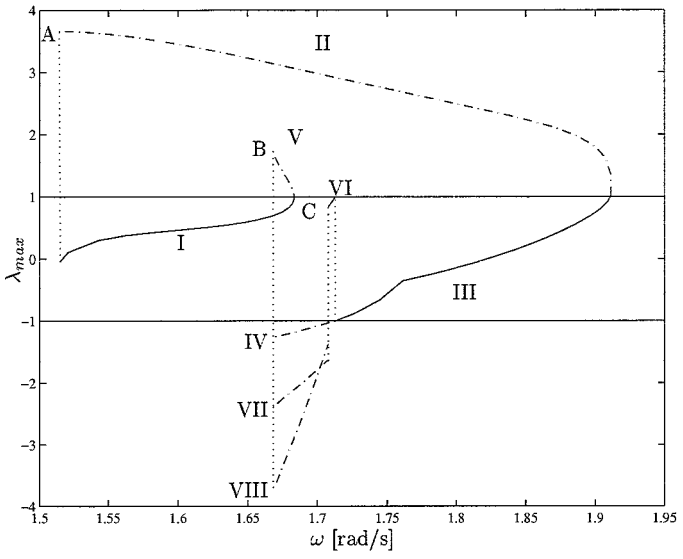

Figure 9.3: Floquet multiplier

the 'full' map will also contain a tent structure.

The *tent map* has been studied thoroughly in literature [7, 14, 24]. The tent map is the non-smooth piece-wise linear version of the logistic map (both non-invertible). The logistic map is smooth and leads to a cascade of period-doublings which is a well known route to chaos. The distance between two succeeding period-doublings is finite for the logistic map. For the tent map however, infinite many period-doublings occur at the same bifurcation value which leads directly to chaos.

The results on the tent map agree with the behaviour at the bifurcation point B. As there are infinite many period-doublings, we also found a period-8 branch (VIII) starting from point B beside the 'expected' period-4 branch (VII). Consequently, there must exist infinitely other unstable branches starting from point B (period-16, 32, 64...). Only branches VII and VIII are calculated because the infinite other branches become more unstable as their period-doubling number increases and the branches become closely located to each other which makes it difficult to find them. These facts agree with the analytical results on the tent map.

The branches VII and VIII connect bifurcation point B with bifurcation point C which is a discontinuous flip bifurcation. The infinite other unstable branches will probably also be located between bifurcation B and C. As follows from the tent map, the system will behave chaotic for ω-values between B and C.

Yoshitake and Sueoka [29] studied the model carefully and showed that the underlying Poincaré map has a tent structure but did not find the branches VII and VIII (or higher period-doublings). Discontinuous fold and flip bifurcations, where the Floquet multipliers jump at the bifurcation point, were found by Yoshitake and Sueoka, a result not found before in literature. However, they did not show how the Floquet multipliers jump which can be explained from saltation matrices and linear approximation as elaborated in this paper. They classified the region between B and C correctly as chaotic and mentioned the similarity with the bifurcations found by Nusse and Yorke [20]. Nusse and York studied discrete dynamical systems with a tent structure and denoted the discontinuous bifurcations they found by 'border-collision bifurcations'. Their numerical calculations only showed stable solutions. They did not give a method to classify discontinuous bifurcations but conclude their paper that this is still an open question. In this paper it is elaborated that the discontinuous bifurcations can be classified by investigating the linear approximation of the Jacobian, fundamental solution matrix or derivative of the map (Section 5).

A discontinuous flip bifurcation was discussed in this section and it was shown that it is related to the one-dimensional tent map. Infinite many branches therefore meet at the same bifurcation

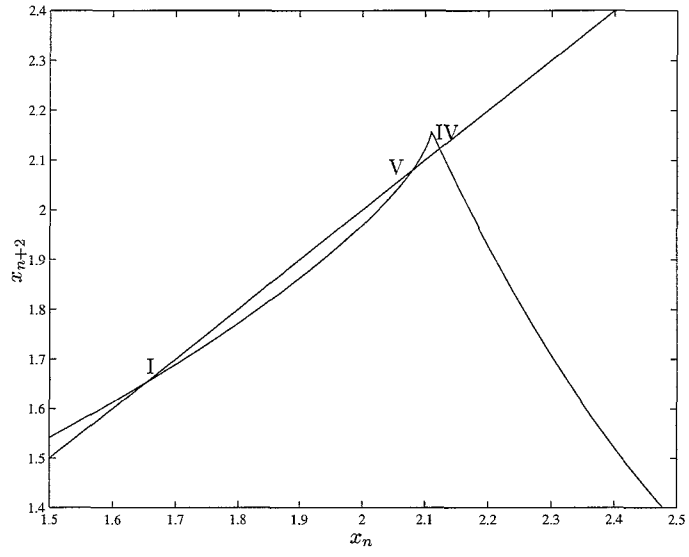

Figure 9.4: Poincaré map ($\omega = 1.67587$ [rad/s])

point and these branches are all period-doublings of the branch under bifurcation. Discontinuous flip bifurcations can collide with fold bifurcations which can yield a bifurcation point where only unstable branches meet.

10 Conclusion

It was shown in this paper that discontinuous vector fields lead to jumps in the fundamental solution matrix if a control parameter is varied. It turned out that a double intersection of a non-smooth hyperplane is necessary to cause a jump of the fundamental solution matrix. These jumps may lead to set-valued Floquet multipliers. A discontinuous bifurcation is encountered if a set-valued Floquet multiplier crosses the unit circle. The periodic solution of a discontinuous system can be transformed to a fixed point of a (locally) continuous but non-smooth Poincaré map. Fixed points of non-smooth continuous systems where discussed and it was shown that for each continuous local bifurcation a discontinuous variant exists.

Continuous as well as discontinuous bifurcations are shown to exist in several discontinuous systems.

An example with a trilinear spring demonstrated two jumps of the Floquet multipliers, one causing a discontinuous fold bifurcation. An example of a stick-slip system showed that the Floquet multiplier can also jump to infinity. The discontinuous fold bifurcation connects a stable branch to an infinitely unstable branch. The unstable limit cycle can be understood by Filippov's theory. Infinitely unstable periodic solutions come into being through repulsion sliding modes and can be found through backward integration. Branches of infinitely unstable periodic solutions can be continued with pseudo-arclength continuation based on shooting with backward integration. Bifurcation to infinitely unstable periodic solutions lead to complete failure of the classical smoothing method to investigate discontinuous systems.

A continuous and a discontinuous symmetry-breaking bifurcation were shown to exist in a mass-spring-damper system with dry friction.

A discontinuous flip bifurcation was discussed by studying a forced block-on-belt system and it was shown that the bifurcation is related to the one-dimensional tent map. Infinite many branches therefore meet at the same bifurcation point and these branches are all period-doublings of the branch under bifurcation. Discontinuous flip bifurcations can collide with fold bifurcations which can yield a bifurcation point where only unstable branches meet.

The *conversion matrix* and *unwrapped fundamental solution matrix* were introduced in this paper as convenient tools to describe saltation of fundamental solution matrices.

Many problems are still open for further research. A discontinuous variant was found for all continuous bifurcations of fixed points, but it was not investigated whether there exists other type of discontinuous bifurcations that cannot directly be classified by a saddle-node, transcritical, pitchfork or Hopf bifurcation.

Only codimension-1 bifurcations were discussed. Further research may extend the theory to codimension-k bifurcations.

The present theory gives a definition of discontinuous bifurcations, incorporating the theory for smooth systems. Much work still has to be done on the numerical aspects of continuation of branches of periodic solutions.

Nevertheless, a theory is presented for local bifurcations of periodic solutions of discontinuous systems.

Appendix A; Stick-slip system

$k = 1$ N/m
$c = 0$ Ns/m in Subsection 4
$c = 0.1$ Ns/m in Subsection 7.3
$m = 1$ kg
$v_{\mathrm{dr}} = 1$ m/s
$F_{\mathrm{slip}} = 1$ N
$F_{\mathrm{stick}} = 2$ N
$\eta = 10^{-4}$ m/s
$TOL = 10^{-8}$

Appendix B; Trilinear system

$m = 1$ kg
$c = 0.05$ N/(ms)
$k = 1$ N/m
$x_c = 1$ m
$k_f = 4$ N/m
$c_f = 0.5$ N/(ms)
$f_0 = 0.2$ N

Appendix C; Forced vibration with dry friction

$m = 1$ kg
$c = 0.01$ N/(ms)
$k = 1$ N/m
$f_0 = 2.5$ N
$F_{\mathrm{slip}} = 1$ N
$F_{\mathrm{stick}} = 2$ N

Appendix D; Forced stick-slip system

$m = 1$ kg
$c = 0$ N/(ms)
$k = 1$ N/m
$v_{\mathrm{dr}} = 1$ m/s
$\alpha_0 = 1.5$ N
$\alpha_1 = 1.5$ Ns/m
$\alpha_3 = 0.45$ Ns^3/m^3
$f_0 = 0.1$ N

References

[1] Aizerman, M. A. and Gantmakher, F. R., 'On the Stability of Periodic Motions', *Journal of Applied Mathematics and Mechanics* (translated from Russian), pp. 1065-1078, 1958.

[2] Andronov, A. A., Vitt, A. A. and Khaikin, S. E., *Theory of Oscillators*, translated from Russian, Oxford, 1966.

[3] Ascher, U. M., Mattheij, R. M. M. and Russell, R. D., *Numerical Solution of Boundary Value Problems for Ordinary Differential Equations.* Society for Industrial and Applied Mathematics, Philadelphia, 1995.

[4] Bockman, S.F., 'Lyapunov Exponents for Systems Described by Differential Equations with Discontinuous Right-Hand Sides', Proceedings of the *American Control Conference*, pp. 1673-1678, 1991.

[5] Filippov, A. F., 'Differential equations with discontinuous right-hand side', *American Mathematical Society Translations*, Series 2, 42, pp. 199-231, 1964.

[6] Galvanetto, U., Bishop, S. R. and Briseghella, L., 'Mechanical Stick–slip vibrations', *International Journal of Bifurcation and Chaos*, **5**(3), 1995, 637-651.

[7] Glendinning , P., *Stability, instablility and chaos: an introduction to the theory of nonlinear differential equations*, Cambridge Texts in Applied Mathematics, Cambridge, 1994.

[8] Guckenheimer, J. and Holmes, P., *Nonlinear Oscillations, Dynamical Systems, and Bifurcations of Vector Fields*,Applied Mathematical Sciences 42, New York, 1983.

[9] Hagedorn, P., *Non-Linear Oscillations*, Oxford Engineering Science Series 10, Oxford, 1988.

[10] Ibrahim, R. A., 'Friction-induced vibration, chatter, squeal and, chaos; Part I: Mechanics of contact and friction', *ASME Applied Mechanics Reviews*, **47**(7), 1994, 209-226.

[11] Ibrahim, R. A., 'Friction-induced vibration, chatter, squeal and, chaos; Part II: Dynamics and modeling' *ASME Applied Mechanics Reviews*, **47**(7), 1994, 227-253.

[12] Kuznetsov, Y. A., *Elements of Applied Bifurcation Theory*, Applied Mathematical Sciences 112, New York, 1995.

[13] Leine, R. I., Van Campen, D. H., De Kraker, A. and Van den Steen, L., 'Stick-Slip Vibrations Induced by Alternate Friction Models', *Nonlinear Dynamics*, **16**, pp. 41-54, 1998.

[14] Martelli, M., *Discrete dynamical systems and chaos*, Pitman Monographs and Surveys in Pure and Applied Mathematics 62, New York, 1992.

[15] Müller, P. C., 'Calculation of Lyapunov Exponents for Dynamic Systems with Discontinuities', *Chaos, Solitons and Fractals*, Vol. 5, No. 9, pp. 1671-1681, 1995.

[16] Natsiavas, S., 'Periodic Response and Stability of Oscillators with Symmetric Trilinear Restoring Force', *Journal of Sound and Vibration*, **134**(2), pp. 315-331, 1989.

[17] Natsiavas, S. and Gonzalez, H., 'Vibration of harmonically excited oscillators with asymmetric constraints', *ASME Journal of Applied Mechanics*, **59**, pp. 284-290, 1992.

[18] Nayfeh, A. H. and Balachandran, B., *Applied Nonlinear Dynamics; Analytical, Computational, and Experimental Methods*, New York, 1995.

[19] Nayfeh, A. H. and Mook, D. T., *Nonlinear Oscillations*, Wiley, New York, 1979.

[20] Nusse, H. E. and York, J. A., 'Border-collision bifurcations including "period two to period three" for piecewise smooth systems', *Physica* D, **57**, pp. 39-57, 1992.

[21] Parker, T. S. and Chua, L. O., *Practical Numerical Algorithms for Chaotic Systems.* Springer-Verlag, New York, 1989.

[22] Popp, K., 'Some model problems showing stick-slip motion and chaos', in *ASME WAM, Proc. Symp. on Friction Induced Vibration, Chatter, Squeal, and Chaos*, Vol. 49, R.A. Ibrahim and A. Soom (eds.), ASME New York, 1992, pp. 1-12.

[23] Popp, K., Hinrichs, N. and Oestreich, M., 'Dynamical behaviour of a friction oscillator with simultaneous self and external excitation', in *Sādhāna: Academy Proceedings in Engineering Sciences*, Indian Academy of Sciences, Banglore, India, Part 2-4, **20**, 1995, 627-654.

[24] Rasband, S. N., *Chaotic Dynamics of Nonlinear Systems*, New York, 1990.

[25] Seydel, R., *Practical Bifurcation and Stability Analysis; From Equilibrium to Chaos*, Interdisciplinary Applied Mathematics, New York, 1994.

[26] Stelter, P., 'Nonlinear vibrations of structures induced by dry friction', *Nonlinear Dynamics*, **3**, 1992, 329-345.

[27] Stelter, P. and Sextro, W.,'Bifurcations in Dynamical Systems with Dry Friction', *International Series of Numerical Mathematics*, Vol. 97, pp. 343-347, 1991.

[28] Van de Vrande, B. L., Van Campen, D. H. and De Kraker, A., 'Some Aspects of the Analysis of Stick-slip Vibrations with an Application to Drillstrings', *Proceedings of ASME Design Engineering Technical Conference*, 16th Biennial Conference on Mechanical Vibration and Noise, DETC/VIB-4109, published on CD-ROM, 8 pp., Sacramento, September 14-17, 1997.

[29] Yoshitake, Y. and Sueoka, A., 'Forced Self-exited Vibration Accompanied by Dry friction', to be published in 'Applied Nonlinear Dynamics and Chaos of Mechanical Systems with Discontinuities', M. Wiercigroch and A. de Kraker (eds.).